AD

EARTHQUAKE ENGINEERING SUPPORT PHASE 2

Final Technical Report

by

R S Steedman

January 1999

United States Army

EUROPEAN OFFICE OF THE U.S. ARMY

London England

CONTRACT NUMBER: N68171-98-C-9014

PRINCIPAL INVESTIGATOR: DR R S STEEDMAN

SUMMARY

This project is a continuation of earlier research work by the Principal Investigator in support of the Earthquake Engineering Research Program, under the direction of the USAE Waterways Experiment Station at Vicksburg, Mississippi. The program of experiments investigating the earthquake behavior and liquefaction of deep sand deposits has generated a large body of data for analysis. This Final Technical Report describes the database that has been developed to date and presents the analysis and the initial conclusions of the study. Data of excess pore pressures at different depths is used to deduce the onset of liquefaction under different initial effective overburden stresses. The object of the research is to compute the factor K_σ, widely used in design calculations to relate the liquefaction resistance at high effective confining stresses to the strength deduced from laboratory experiments at 1 tsf. By comparing the data obtained from the centrifuge experiments with standard design approaches for the prediction of liquefaction, an assessment of the relationship between K_σ and depth can be made. This is discussed and areas where further experimental work is required are highlighted. The results are also presented in the form of log-log (stress focus) plots and compared with laboratory element test data. Preliminary conclusions indicate that the centrifuge data more closely match relationships based on field experience than laboratory data.

LIST OF KEYWORDS

liquefaction
centrifuge
earthquake
model
experiment
sand

TABLE OF CONTENTS

LIST OF APPENDICES

1.0 INTRODUCTION

This research contract addresses the second phase in the completion of an experimental and analytical research programme in support of the Earthquake Engineering Research Program under the direction of the USAE Waterways Experiment Station, Vicksburg, Mississippi and is a continuation of earlier research under Contract Nos. N68171-97-M-5710 and N68171-97-C-9012. During this period of research the principal activity has been to extend the series of liquefaction experiments into a higher range of initial effective overburden stress, to complete the processing of all experimental data and to complete the initial analysis of the database.

The prediction of the strength of soil at the onset of liquefaction, termed the liquefaction resistance, as a function of confining pressure has historically been based on laboratory element test data. With increasing initial effective confining pressure, laboratory element tests indicate a reduction in the cyclic strength or liquefaction resistance of the soil, as a non-linear function of the confining stress.

More recently, in situ test correlations have been developed based on in-situ measurements, such as the SPT, cone penetrometer test or shear wave velocity measurement. However, the data-base against which such correlations may be made is limited to relatively low vertical effective stresses, and laboratory element tests are still required to extrapolate these correlations to higher effective confining stresses more typical of many field design problems.

The selection of the factor defining the ratio of the cyclic resistance ratio at any stress to the cyclic resistance ratio at 1 atm, defined as K_σ, is critical to the assessment of the strength of existing or proposed structures. Too low, and unnecessary additional strengthening work may be specified. Too high, and the structure may pose an unacceptable risk of catastrophic failure.

In this study, centrifuge earthquake model test data are used to compare with laboratory and field test data of the onset of liquefaction in clean fine sand over a wide range of effective confining stresses and at varying density and overconsolidation ratio.

This Final Technical Report for Phase 2 of the work presents the data-base as it had been developed by the end of December 1998 and describes the initial calculations of the K_σ factor, using the methods proposed under Phase 1. These are discussed in detail below.

The analysis follows standard design procedures to normalise the data so that comparisons may be made with published results from laboratory element tests. The analysis makes use of the concept of stress focus, Hynes (1998), by which strength data are plotted in log-log space as a function of effective confining stress and from which trends with confining stress may be more easily identified than in the standard representations.

2.0 SUMMARY OF CENTRIFUGE EXPERIMENTS

Series 1 comprised a series of experiments investigating the liquefaction of a loose saturated layer under varying effective overburden pressures. The aim of the experiments was to achieve an improved understanding of the K_σ factor in liquefaction analysis through centrifuge model tests of a level, saturated sand bed under strong base shaking. Each centrifuge experiment generated a large body of data from instrumental records, from measurements made during construction and excavation, from photographs, video records and other sources.

The models under Series 1 were designed based on a target effective overburden stress in the middle of the loose layer. Instrumentation at other depths was intended to capture data of the onset of liquefaction under different levels of vertical effective stress in the same experiment. However, these higher elevations in the specimen were often affected by the response of layers below. The importance of the target elevation in the middle of the loose layer was that a fixed volume of sand of similar relative density lay below.

	Models 1, 2	**Model 3**	**Model 4**	**Model 5**
Description	Saturated, level sand bed with 160 mm deep loose layer at the base of the model	Saturated, level sand bed with 160 mm deep loose layer at the base of the model	Saturated, level sand bed with 160 mm deep loose layer at the base of the model and a depressed phreatic surface	Saturated, level sand bed with a 160 mm deep loose sand layer overlain by a layer of denser sand, and surcharged
Surcharge pressure	none	none	none	upto 15.4 KPa (2.23 psi)
Sand dry density (upper layer)	1672 kg/m^3 (104.4 pcf)	1672 kg/m^3 (104.4 pcf)	1672 kg/m^3 (104.4 pcf)	1672 kg/m^3 (104.4 pcf)
Sand dry density (loose layer)	1611 kg/m^3 (100.6 pcf)	1611 kg/m^3 (100.6 pcf)	1611 kg/m^3 (100.6 pcf)	1611 kg/m^3 (100.6 pcf)
Pore fluid	glycerine-water	glycerine-water	glycerine-water	glycerine-water
Viscosity	50 cS	50 cS	50 cS	50 cS
g level at 6 m	50	50	50	50
Thickness of upper sand layer	140 mm	365 mm	365 mm	365 mm
Depth of phreatic surface	0 mm	0 mm	365 mm	0 mm
Target effective vertical stress at g	107 KPa (1 tsf)	215 KPa (2 tsf)	320 KPa (3 tsf)	upto 980 KPa (9.2 tsf)
Total depth of model	300 mm	525 mm	525 mm	525 mm + surcharge
Total mass of specimen (excl box)	330 kg (est)	575 kg (est)	508 kg (est)	1315 kg (varies)

Table 2.1 Summary of model designs under Series 1

The experiments were divided into classes of model, denoted Models 1 through 5 as shown in Table 2.1. Each class of model reflected a different target effective overburden stress. (Model 2 was identified as a separate class of model from Model 1 because the sand used in Model 2 was

different.) The suffix a, b, c indicates successive repeats of that particular model, or a very similar design.

The materials used in the model were characterised by standard laboratory tests to determine parameters such as dry density and gradation. The properties of Ottawa sand, Nevada sand and glycerine (mixed with water and used as the pore fluid) are given in Tables 2.2, 2.3, 2.4.

Specific gravity	2.68
Maximum void ratio	0.7633
Minimum void ratio	0.4762
D_{50}	0.12 mm (approx)
D_{10}	0.075 mm (approx)

Table 2.2, Ottawa Sand specification

Specific gravity	2.64
Maximum void ratio	0.757 (density 93.8 pcf)
Minimum void ratio	0.516 (density 108.7 pcf)
D_{50}	0.18 mm (approx)
D_{10}	0.11 mm (approx)

Table 2.3, Nevada Sand specification

The pore fluid comprised a mixture of glycerine and water, 80% by weight for experiments conducted at 50g. Measurements of the viscosity of glycerine-water mixes at a range of temperatures and proportions showed that the viscosity was sensitive to both parameters, Table 2.5. A full presentation of the results of viscosity measurements as a function of temperature is given in Appendix A. The density of a glycerine water mix is calculated from :

$$\rho_m = \rho_g(m_g + m_w)/(m_g + \rho_g\, m_w)$$

where ρ_m is the density of the mix, ρ_g is the density of glycerine, m_g is the mass of glycerine, and m_w is the mass of water.

Density	1200 kg/m^3 (80% by weight)
Viscosity	50 cS
Specific Gravity	1.26
Composition	80% glycerine-water mix (by weight)

Table 2.4 Specification for pore fluid

The models were poured dry from a hopper and saturated under vacuum, or occasionally under gravity. Instrumentation would be placed in the model as it was being constructed.

% glycerin by weight	Viscosity (cS) at temperature (deg C)		
	20	**25**	**30**
0	0.98	0.89	0.82
50	8.46	6.47	4.84
65	18.37	16.48	14.93
75	39.77	30.28	23.06
85.6	102.10	75.26	55.48

Table 2.5 Viscosity of glycerine (as measured)

Model Code	WES CRC Ref.	Overall Depth (mm)	Relative Density	σ_v' (tsf)	Date	Eqs	Comments
						oc =	overconsolidated
1a	1	300	52% loose 70% dense	1	4/12/97	2	Cambridge ESB
2a	2	300	44% loose 83% dense	1	20/2/98	3	Cambridge ESB. PPTs not recorded
2b	5	300	50% loose 75% dense	1	30/4/98	2	ESB #1. Liquefaction after around 11 cycles in eq1
2c	8	300	49% loose 74% dense	1	6/6/98	5	ESB #1. Low amplitude input. Slow rise in ppts
2d	9	300	50% loose 75% dense	1	12/8/98	4	ESB #2. Liquefaction after around 7 cycles in eq1
2e	10	300	49% loose 73% dense	1	26/8/98	4oc	ESB #1. Good definition in loose layer, 13 cycles
2f	14	300	50% loose 75% dense	1	22/9/98	4oc	ESB #1. Liquefaction throughout. High quality
3a	3	525	34% loose 73% dense	2	30/3/98	2	Cambridge ESB. Spikey input. Rapid rise time
3b	6	525	49% loose 77% dense	2	1/5/98	3	ESB #2. No data eq1, good data liquefaction eq2
3c	7	525	49% loose 79% dense	2	5/5/98	3	ESB #2. Rapid onset liquefaction eq1 and eq2
3d	11	525	54% loose 80% dense	2	3/9/98	4oc	ESB #2. Linear rise, good definition liqn in loose layer
4a	12	525	49% loose 78% dense	3	14/9/98	4	Saturated to top of loose layer. ESB #1. Liquefied at base only, eq1 after 25 cycles
4b	13	525	56% loose 74% dense	3	15/9/98	4oc	Saturated to top of loose layer only. ESB #2. No pore pressure rise eq1, some eq2
4c	17	525	50% loose 75% dense	4.7	22/10/98	4	Surcharge, ESB #1. Strong rise at base, probable arching
4d	18	525	50% loose 68% dense	4.7	4/11/98	5oc	Surcharge, ESB #1. Strong rise to 100% at base, arching
5a	15	525	51% loose 72% dense	7.4	7/10/98	4	Surcharge, ESB #1. Liquef'n at base, arching reduced σ_v'
5b	16	525	49% loose 76% dense	7.4	14/10/98	4oc	Surcharge, ESB #1. Liquef'n at base, arching reduced σ_v'
5c	19	525	52% loose 75% dense	9.1	11/12/98	3	Surcharge, ESB #2. Low level of excess pp

Table 2.6 Summary of centrifuge experiments, Dec 1997 – Dec 1998

To facilitate the interpretation of the experimental data, a factual data report was completed for each experiment. This recorded the nature of the model, and details of the instrumentation layout and calibrations.

All data was processed into engineering units and checked for obvious sources of error (earthing problems, electrical spikes, low signal to noise ratio). Offsets were removed using the average of the first 200 points (typically).

In the period December 1997 to December 1998 eighteen model experiments and 64 earthquakes were completed. All models, with the exception of Model 1a, were constructed from Nevada sand. Model 1a was constructed from Ottawa sand. The experiments analysed for this report are summarised in Table 2.6 .

A schematic cross-section through a typical shallow (300 mm) model, Model 2b, and a typical deep (525mm) model, Model 3c, is given in Figures 2.1 and 2.2.

Typical earthquake time histories from Model 3c are illustrated in Figure 2.3, which shows the base shaking motion, motion at the middle of the loose layer, motion near the surface, as well as the excess pore pressure response at two depths in the specimen for the first earthquake, EQ1. Figure 2.4 presents the same information for the second earthquake, EQ2.

Using harmonic wavelet analysis, time-frequency 'maps' can be generated from the time histories of acceleration recorded in the models. Newland and Butler have described the wavelet approach to the study of transient signals from centrifuge models in recent papers, Newland and Butler (1998, 1999). Figure 2.5 shows the time-frequency map for the base input motion ACC12609 throughout the earthquake, compared with the time-frequency map for ACC12610, in the middle of the liquefying loose layer.

During the early stages of shaking, there is a rapid increase in excess pore pressure and consequent reduction in soil stiffness. This takes place between about 0.17 and 0.27 seconds in earthquake 1, and 0.2 and 0.3 seconds in earthquake 2. Time-frequency maps for these stages are shown in Figures 2.6 and 2.7 respectively. In these plots, the excess pore pressure and the base acceleration are also reproduced, to the same time scale, so that a direct comparison may be made. It is clear that during this period there is a reduction in at least one of the main resonance frequencies in the specimen, from around 90 to around 85 Hz. This frequency corresponds roughly to the third harmonic of the input frequency (27 Hz) and also to the likely combined soil and container fundamental mode.

In both EQ1 and EQ2 a sharp rise in the energy at around 140 Hz takes place almost exactly coincident with excess pore pressure reaching 100%. This is an interesting result which warrants further research. 140 Hz is near the fifth harmonic of the input shaking. Examination of the time histories in Figures 2.3 and 2.4 showed sharp spikes developing in the acceleration record as the soil around the accelerometer liquefies. The physical explanation of this is more complex. It may be associated with transient

shock waves 'locking up' the soil instantaneously and then 'releasing' it again. If the shock wave was generated by the fundamental shaking motion of the specimen, then this would explain why the high frequency spike only occurs on each half cycle of base motion. Alternatively, it may be associated with a fracture type phenomenon as the soil liquefies and high frequency energy is generated. Further work on this is necessary.

Additional insights may be gained by subtracting the absolute values of two harmonic wavelet transforms to give a differential plot. This gives a comparison of the energy at different locations in the model. Figures 2.8 and 2.9 show differential plots for accelerometers 12609 and 12610 in Model 3c, earthquakes 1 and 2 respectively. The intense band along the base of the two figures shows that the input shaking energy is much greater at the base of the model than in the middle of the loose layer (ACC12610), as expected. However, energy at around 84Hz was amplified between the base of the sand bed and the middle of the loose layer, a small distance above. Here the absolute value of the differential is negative. This effect was transient in earthquake 1, decaying with time, but was relatively uniform throughout the duration of earthquake 2, possibly even building up during the second half of the shaking.

3.0 STRESS HISTORY

The stress history at the location of each transducer was calculated using a time history of acceleration. One accelerometer record was selected based on the quality of its signal and its location. Generally the device was located on the bottom ring of the ESB, but occasionally the accelerometer at the base of the sand specimen was used instead. In some cases, where amplification was considered significant, an amplification analysis was carried out by examining the peak acceleration at different elevations in the model, based on the very early cycles of shaking before significant degradation had taken place. The mean of positive and negative cycles was used, and commonly high frequency spikes were removed by smoothing where these were considered to be unrepresentative of the character of the motion. Plotting amplification as a function of the base input motion revealed that generally the amplification was around 1.

The cyclic stress ratio at any depth was calculated as follows.

The method used was that originally proposed by Seed and Idriss (1971) and developed by Ishihara (1996). It is based simply on using the ground acceleration to predict the stress history at any depth using the following relationship :

$$\frac{\tau_{max}}{\sigma'_v} = \frac{a_{max}}{g} r_d \frac{\sigma_v}{\sigma'_v}$$

where a_{max} is the acceleration at the ground surface and $\tau_{max} = \tau_{hv,c,max}$ is the shear stress on a horizontal plane. The reduction factor r_d may be taken as $r_d = 1 - 0.015\ z$ (z is the depth in metres), Iwasaki et al. (1978). The ground surface acceleration time history in the centrifuge specimen is frequently distorted by the liquefaction in the soil strata beneath, which often isolates the surface from the underlying motion. So the base input motion was used, scaled using an amplification factor derived from the actual profile of amplification observed in the specimen (described above).

In practice, the following steps were taken. The base input acceleration record and amplification factor were selected. The depth of each pore pressure transducer was established from the Factual Report and its static reading before (or in some cases after) the earthquake was used to compute the depth of fluid above the device. The total vertical stress at each depth was calculated from the as-placed density values for the soil above the device and the weight of fluid or surcharge on the surface. The effective vertical stress was calculated.

The peak excess pore pressure was calculated as a percentage of the effective vertical stress. In certain cases, where arching was suspected (as liquefaction had taken place without the excess pore pressure reaching 100% of the initial vertical effective stress), an adjustment was made to the total stress to raise the percentage of the excess pore pressure to around 100%. This reduced the effective vertical stress to a new value, which was the value subsequently used in the database of stress ratio and effective overburden stress.

The shear stress history at each depth as a function of effective vertical stress was calculated by multiplying the earthquake acceleration ratio by the calculated reduction factor and the ratio of effective vertical to total vertical stress. The maximum cyclic stress ratio was found, by taking the mean of the maximum positive and negative values. Maximum stress ratios were calculated based on both 'raw' and 'smoothed' accelerometer time histories. The smoothing function generated a new value at each time step, based on ¼ of the previous point, ½ of the current point and ¼ of the next point. The smoothed maximum cyclic stress ratio was factored by 0.65 following conventional practice to give the cyclic stress ratio at each pore pressure transducer depth.

The pore pressure records were then examined to determine the onset of liquefaction. This was taken as the point at which the residual excess pore pressure reached a limiting value. Many records showed a cyclic response during pore pressure buildup, and the peak pore pressure would reach the ultimate limiting value significantly before the residual. In these cases, accelerometer records would be examined to determine whether there was any significant change in their response which could be used as a further indication of the onset of liquefaction. It was concluded that the time at which the residual pore pressure reached the limiting value was the most consistent and reliable definition. This point was estimated by eye and the process is illustrated in Figure 3.1 and Table 3.1 using data from Model 3c, earthquake 1. Using the period associated with the dominant frequency of shaking, the number of 'cycles' to reach liquefaction was calculated based on the time and the dominant period of earth shaking.

Actual depth (mm)	Prototype depth (m)	Static pore pressure at 50g (KPa)	Depth fluid on surface (m)	Total vertical stress, σ_v (KPa)	Effective vertical stress, σ'_v (KPa)
439	21.95	263	0.39	457	194
Maximum cyclic stress ratio (raw)	Maximum cyclic stress ratio (smoothed)	Cyclic stress ratio τ/σ'_v	Effective vertical stress (tsf)	Onset of liquefaction (seconds)	Number of cycles equivalent (N)
0.246	0.239	0.155	1.8	0.308	4.27
Data for :	**Model 3c**				
G level	Saturated unit weight (dense)	Saturated unit weight (loose)	Fluid unit weight	Earthquake start (seconds)	Frequency (Hz)
50 g	20.7 KN/m³	20.2 KN/m³	11.8 KN/m³	0.15	27

Table 3.1 Base data and calculations of stress ratio and number of cycles to liquefaction for PPT30, Model 3c, earthquake 1 (refer also to Figure 3.1)

This process was repeated across all transducers and models to build the database attached as Appendix B. The data were segregated by density, first and following earthquakes, normally or overconsolidated. Each datapoint was then reviewed and a quality rating attached to it, ranging from * for top quality, through high, medium and low. The reasons for the rating are presented in the database. The rating would be reduced for reasons such as uncertainty over the timing of the onset of liquefaction, high frequencies

distorting the accelerometer records, uncertainty over the static pore pressure values. Figures 3.2, 3.3, 3.4, 3.5, 3.6, 3.7 present the data of * and high rating only.

The next stage was to calculate K_σ. To normalise the data at 10 cycles it was first necessary to select a standard curve or family of curves which best represented the trend of the data, starting first with the normally consolidated 50% RD data (shown in Figure 3.2). Using reference data reproduced by Youd and Idriss (1997), curves were developed which best matched the 'factors' scaling the cyclic stress ratio to cause liquefaction in 15 cycles to any other number of cycles. These are reproduced in Appendix C. The original Seed and Idriss values generate a 'flat' curve represented by the function $F = 5.24\ N^{-0.61}$. Proposals by Ambraseys can be represented by a relatively steep curve matched by the function $F = 3.48\ e^{-0.08\ N}$. A more recent proposal by Idriss (Youd and Idriss, Table 3) yields a steeper curve, represented by the function $F = 3.47\ N^{-0.45}$. Using these functions a family of curves can be drawn as a function of the number of cycles by choosing an arbitrary range of stress ratios at 15 cycles and computing the curves which pass through them. Figures 3.8, 3.9 and 3.10 show the family of curves generated by the Seed and Idriss factors, the Ambraseys factors and the Idriss factors compared with the centrifuge data of normally consolidated 50% RD, first earthquake specimens. It is clear that the data are best matched by the Idriss factors (of the three choices), although a slightly flatter curve may match the data even more closely (WES curve in Appendix C).

Using the Idriss curve function, the least squares best fit curve to the data at 1 tsf was found, and this is shown in Figure 3.10. This was found by iteration, varying the stress ratio at 15 cycles until the optimum curve through the data points was identified. This curve was found to pass through a stress ratio of 0.1093 at 15 cycles, based on the four data points to date.

Using the same family of curves, each data point was then scaled to its equivalent stress ratio at 10 cycles. As

$$(\tau/\sigma'_v)_N = (\tau/\sigma'_v)_{N=15} \cdot A\ N^{-B}$$

where A and B are the factors describing the family of curves, and therefore

$$(\tau/\sigma'_v)_{N=10} = (\tau/\sigma'_v)_{N=15} \cdot A\ 10^{-B}$$

then

$$(\tau/\sigma'_v)_{N=10} = (\tau/\sigma'_v)_N \cdot 10^{-B} / N^{-B}$$

The ratio of the equivalent cyclic stress ratio at ten cycles (defined as the liquefaction cyclic resistance strength ratio CRR) to the cyclic stress ratio at 10 cycles for the best fit 1tsf curve was calculated, giving K_σ, as shown in Figure 3.11. The open circles are all the * and high quality rating data from the normally consolidated, 50%RD first earthquake centrifuge data. Figure 3.11 also includes data of K_σ calculated by Hynes and Olsen from laboratory test data of Vaid on Tailings sand and Ottawa sand. The curves shown in the figure were calculated using Olsen's function $K_\sigma = (\sigma'_v)^{f-1}$, Olsen (1984).

These data were then replotted in stress focus plots in Figure 3.12. Two curves, representing f = 0.7 and f = 0.95 were drawn through the CRR at 1 tsf (For the centrifuge data, this was the best fit value. For Vaid's data, this was the 1 tsf value.) Also shown in the figure are laboratory test data carried out by Earth Technology Corporation for the VELACS project.

The laboratory test data were processed as follows. Seven experiments were identified from the VELACS data, three undrained cyclic triaxial tests (CIUCyclic) and four undrained cyclic simple shear tests (CSS). These were conducted on sand at 60% RD. Appendix C shows the calculation stages and the original data results. The base data from the experiments was converted to cyclic stress ratio. In the case of the triaxial data, this was converted to a simple shear equivalent using a factor of 2/root3 x q/2 /σ'_3, following Castro. The data was then further adjusted for relative density using the Holtz and Gibbs relation for SPT and relative density for coarse sand. At 1 tsf, the number of blows at 50% RD is around 10. At 60%, this rises to around 13.4. From Seed's figure for a Magnitude 7.5 earthquake the CSR at 50% is around 0.102 and at 60% is around 0.14. hence the data is scaled by a factor of 0.729. Finally, the data was extrapolated to the equivalent CSR at 10 cycles. This was done using both the Idriss curve and the flatter Seed curve. It was found that the flatter Seed curves collapsed the laboratory data on top of the centrifuge data much more closely than the Idriss curve (which more closely reflected the centrifuge data). These laboratory test data for Nevada sand were then plotted in Figure 3.12, using solid squares for the triaxial data and open diamonds for the simple shear data.

The comparison between the (corrected) laboratory data and the Seed and Idriss curves are shown in Figures 3.13 and 3.14 (3.14 shows the results at less than 30 cycles).

Figures 3.15 and 3.16 present the centrifuge and (corrected) laboratory data and omit the Vaid data. In these figures, however, the data from the 75% RD normally consolidated, first earthquakes has also been included (solid squares). This data was processed simply using the Idriss curves and extrapolated to find the value of CSR at 10 cycles using the calculation described above. As with the 50% RD data, only the * and high quality data were used. The data appear to lie on top of the 50% RD data although no correction has been made for relative density.

Finally, a comparison was made between normally consolidated and overconsolidated specimens. Figures 3.17 and 3.18 present the (corrected) laboratory data on Nevada sand together with data from centrifuge experiments on normally consolidated and overconsolidated specimens. An Olsen value of 0.7 was used again to characterise the broad trend of the data. The overconsolidated data appear to lie slightly to the right of the normally consolidated results, indicating a higher cyclic resistance, but the trend with increasing effective confining stress is similar.

4.0 REDUCTION OF STRENGTH WITH INCREASING CONFINING STRESS

Reduction in strength with increasing confining stress is a well established phenomenon. To contrast the reduction in strength computed as a result of liquefaction with the reduction in strength during drained shearing simply associated with the suppression of dilatancy, an analysis following Bolton (1986) was carried out.

Bolton analysed an extensive data-base of laboratory data on the shearing of sands, and concluded that a relationship could be developed between density and confining pressure which enabled the peak secant angle of shearing resistance, ϕ'_{max}, to be predicted directly, based on knowledge of the critical state angle of shearing resistance, ϕ'_{crit}.

Using the relative density $I_D = (e_{max} - e)/(e_{max} - e_{min})$, Bolton defined a relative dilatancy index I_R, where

$$I_R = I_D (10 - \ln p') - 1$$

and in plane strain, $\phi'_{max} - \phi'_{crit} = 5\ I_R$ degrees, in the range $0 < I_R < 4$. The mean effective confining stress $p' = (1 + 2K_o)/3\ \sigma_v'$, where K_o is the coefficient of lateral earth pressure at rest. Using the simple approximation $K_o = 1 - \sin \phi'$, then for $\phi' = 30$ degrees, $p' = 2/3\ \sigma_v'$.

I_R may then be calculated for any value of effective vertical stress and relative density. Using the Mohr circle representation, $\tau/\sigma_v' = \tan \phi'_{max}$. Then, by calculating the value of τ/σ_v' at 1 tsf and comparing it to the values of τ/σ_v' at higher confining stresses, it is possible to compute a K_σ value which is directly comparable to the K_σ values computed from the liquefaction test data. This gives a measure of the reduction in shear strength to be expected as effective confining stresses increase, simply as a result of the suppression of dilatancy. Using a value of $\phi'_{crit} = 30$ degrees (typical for Ottawa sand, following Bolton), then Table 4.1 was developed.

σ_v' (tsf)	(KPa)	I_R (I_D=50%)	ϕ'_{max} (deg)	τ/σ_v'	K_σ
1	107	1.87	39.3	0.819	1
2	215	1.52	37.6	0.770	0.940
4	429	1.17	35.9	0.722	0.882
6	644	0.969	34.8	0.696	0.850
8	858	0.825	34.1	0.678	0.827
10	1070	0.714	33.6	0.664	0.809

Table 4.1 K_σ static, drained shearing

Using higher values of ϕ'_{crit}, upto 35 degrees, shows insignificant changes in the value of K_σ calculated in this manner. Thus these results may be considered to have general application across a range of sands. The results confirm that as a minimum, K_σ should be expected to fall to near 0.8 at 10 tsf effective vertical confining stress even under simple drained shearing

conditions. Vaid's data on Ottawa sand, shown in Figure 3.11, show values close to these in Table 4.1, which is surprising as his data was based on laboratory liquefaction tests and might have been expected to show a value of K_σ lower than the static drained shearing value. Figure 4.1 compares the 'static' K_σ with the curves suggested by Olsen (1984) based on a stress exponent f. The static shear K_σ are matched reasonably well by a factor f = 0.9 in the Hynes and Olsen stress focus representation. This may then be taken as an upper limit on the value of f.

5.0 FURTHER EXPERIMENTS

The range of models used in the first series has encompassed a wide range of effective overburden stresses. The analyses have shown that the data from the centrifuge specimens is directly relevant to the study of K_σ. Issues which need to be addressed in further experimental work include the following:

a) Further experiments are necessary at 1tsf, both normally and overconsolidated. These experiments should include a range of input amplitudes, such that further data of liquefaction in the 10 – 25 cycle range is achieved.

b) The use of surcharges which are comprised of pellets, rather than plate, should be considered. Arching has clearly been observed in several models, and although this does not invalidate the experiment (as the effective overburden stress at the onset of liquefaction can be deduced from the excess pore pressure), it has meant that few data points have been achieved at very high effective stresses.

c) The large depth of the centrifuge specimen means that there is scope for redistribution of excess pore pressure in the model (as in the field situation). This has an important bearing on the timing of the onset of liquefaction in any layer in the specimen, because of the development of excess pore pressure in layers below. In some cases, liquefaction in the upper denser layer has been clearly observed to take place after the end of earthquake shaking. The K_σ approach assumes that layers act independently, and that liquefaction of one layer is unrelated to the response of others. This is clearly not the case in practice, and in field design cases care must be taken to ensure that in assessing the response of any single soil layer, the $K_\sigma$approach is not used in isolation without also considering the effect of adjacent layers.

d) In the light of c) above, there is a strong argument to adopt a uniform density for future specimens. Cases have been observed where the lower loose layer has appeared to influence the onset of liquefaction in the upper layer and where the lower layer has not appeared to affect the response of the upper layer. However, unless the upper layer is modified to a composition that can be certain to be unaffected by the lower layer, then it may be more appropriate, from the point-of-view of interpreting the soil response, to adopt a single 50% Relative Density throughout.

6.0 CONCLUSIONS

a) The first full year of experimental studies has generated a large and valuable data-base of the onset of liquefaction in a saturated sand bed under low to medium effective overburden stresses.

b) The data-base has been analysed using standard approaches to deduce the factor K_σ, which is considered to represent the reduction in liquefaction resistance with increasing effective confining stress. These results have been compared with results from standard laboratory test data of the same sand.

c) Harmonic wavelet analysis of the degradation of soil stiffness with increasing excess pore pressure shows interesting characteristics which require further study, particularly the rapid rise in energy at high frequency coincident with the achievement of initial liquefaction (excess pore pressure reaching 100% of the initial effective vertical stress).

d) The stress focus representation developed by Olsen provides a good tool for studying trends in the data, and for comparisons between different densities and methods of testing.

e) In comparisons with standard curves representing the relationship between cyclic stress ratio and number of cycles to liquefaction, developed from laboratory element test results and used in conjunction with estimates of the number of equivalent cycles in earthquakes of varying magnitude, it appears that the centrifuge data more closely reflect experience from the field, rather than the laboratory. In particular, it was found that the Magnitude Scaling Factors proposed by Idriss in his H B Seed Memorial lecture were a closer match to the data than the original Seed and Idriss factors, or than other proposals, such as those of Ambraseys, or Youd and Noble.

f) Analysis of the reduction of shear strength as a result of the suppression of dilation has shown that K_σ should reduce to a value of around 0.8 at 10 tsf even under drained static shearing conditions. This is close to an Olsen value of 0.9, which may then be considered to be an upper bound on K_σ. The fact that some laboratory test data lie above this value suggest that other factors may be affecting the strength results deduced from the element tests.

REFERENCES

Bolton M D (1986) The strength and dilatancy of sands, Geotechnique 36, No. 1, pp 65-78.

Hynes M E (1998) Influence of confining stress on liquefaction resistance, Proc Int Workshop on the Physics and Mechanics of Soil Liquefaction, Baltimore, MD, 10-11 Sept 1998, A A Balkema.

Newland D E and Butler G D (1998) Application of time-frequency analysis to strong motion data with damage, Proc 69th Shock and Vibration Symp, Session HB1, SAVIAC, Minneapolis.

Newland D E and Butler G D (1999) Time-varying cross-spectra for soil motion with damage, 17th ASME Biennial Conference on Mechanical Vibration and Noise, Proc 1999 ASME Design Engineering Tech Conf, Sept 12-15, Las Vegas.

Olsen R S (1994) Normalisation and prediction of geotechnical properties using the Cone Penetrometer Test (CPT), PhD Dissertation, University of California, Berkeley.

PHRI (1997) Handbook on liquefaction remediation of reclaimed land, Balkema.

Seed R B and Harder L F (1990) SPT-Based analysis of cyclic pore pressure generation and undrained residual strength, Proc. H Bolton Seed Memorial Symposium, Vol. 2, pp 351 - 376, BiTech Publishers Ltd, Vancouver.

Steedman R S (1997) Development of a Centrifuge Model Test Program for the study of liquefaction, Final Technical Report, European Research Office of the US Army, London, Contract N68171-97-C-9012.

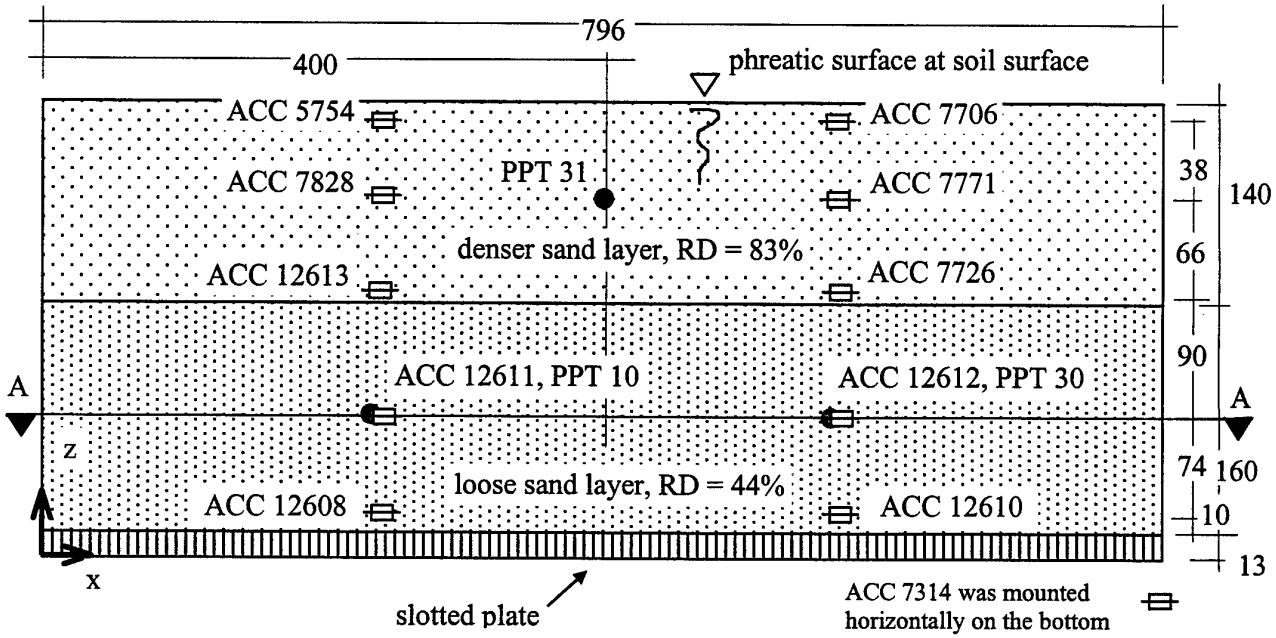

Cross-section through Model 2b

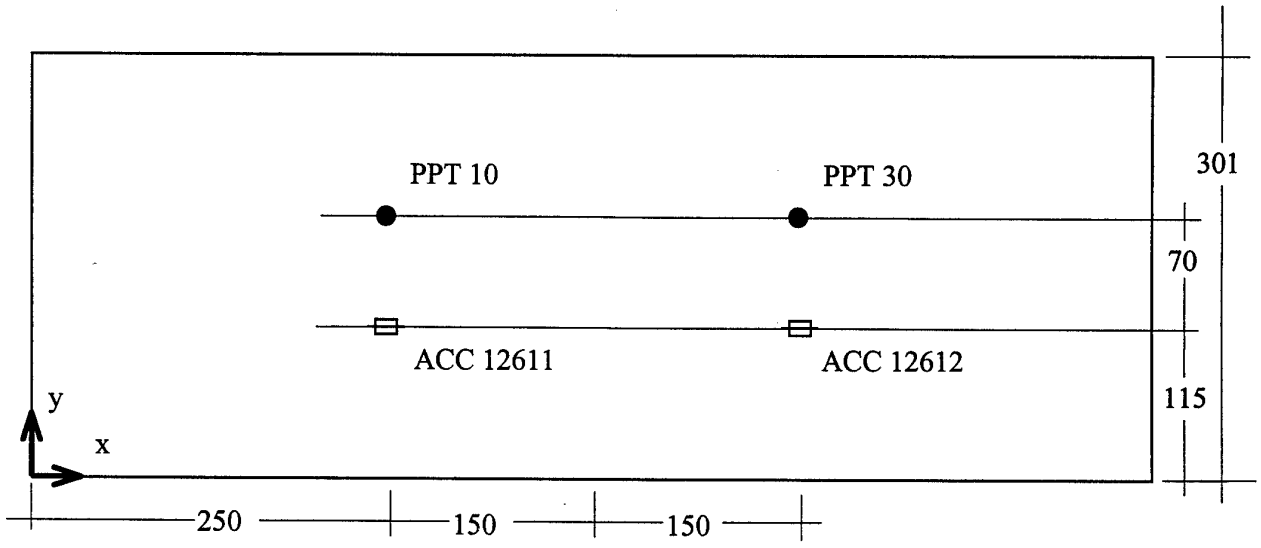

Plan on section A-A showing locations of transducers at mid-depth in the loose layer

Note: exact coordinates of all transducers (measured before and after the experiment) are listed in the Factual Report.

Figure 2.1 Model 2b, location of transducers

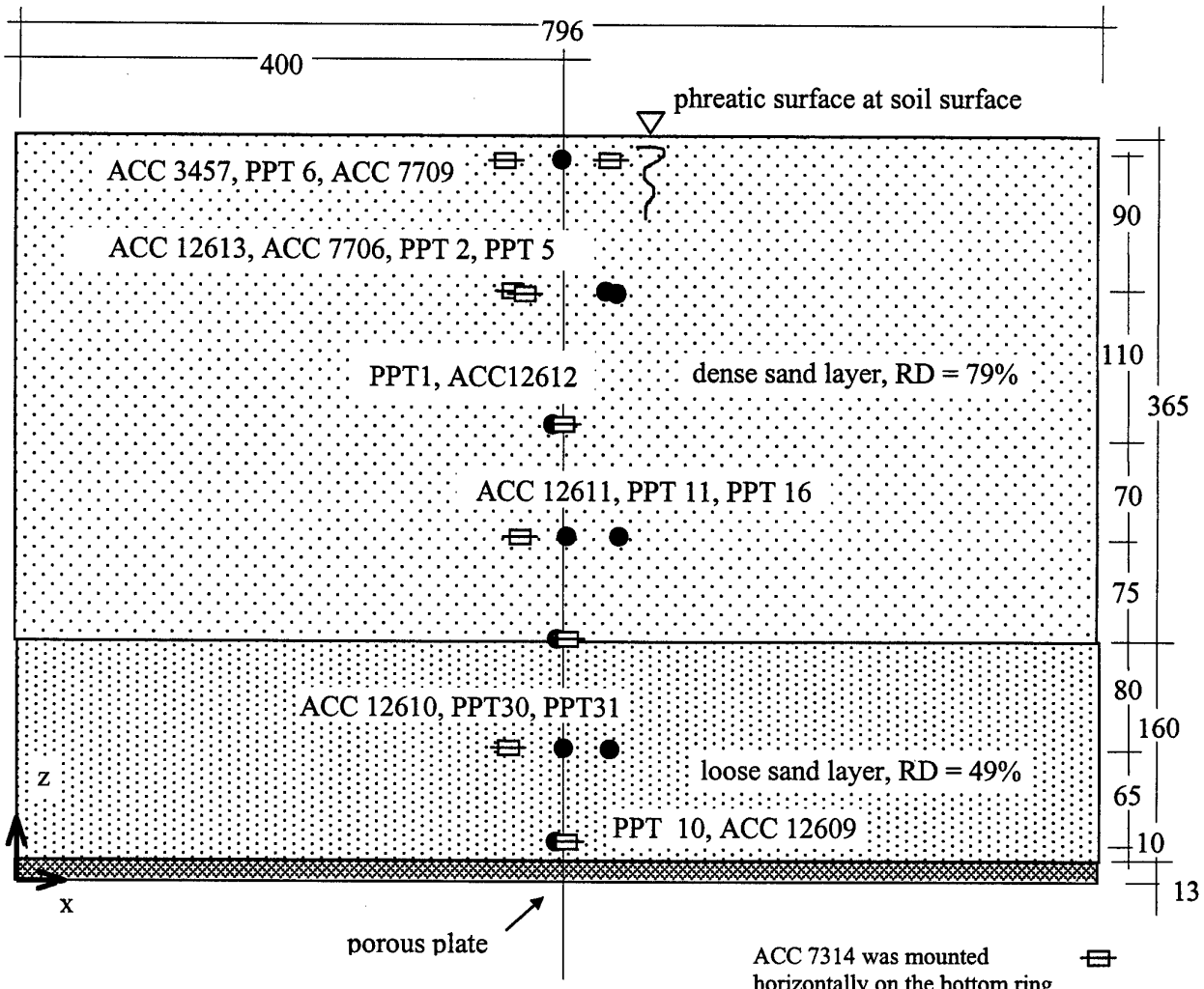

Cross-section through Model 3c

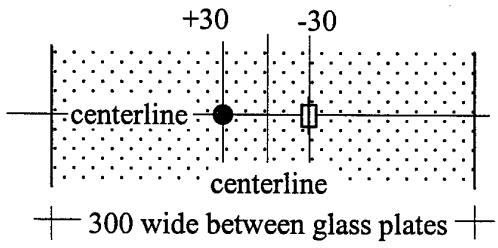

Plan at level with two transducers

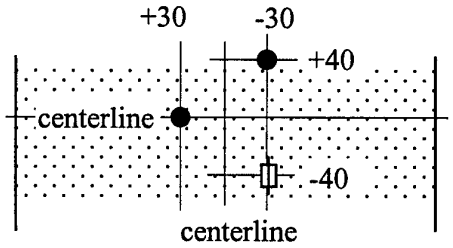

Plan at level with three transducers

Note: exact coordinates of all transducers (measured before and after the experiment) are listed in the Factual Report.

Figure 2.2 Model 3c, location of transducers

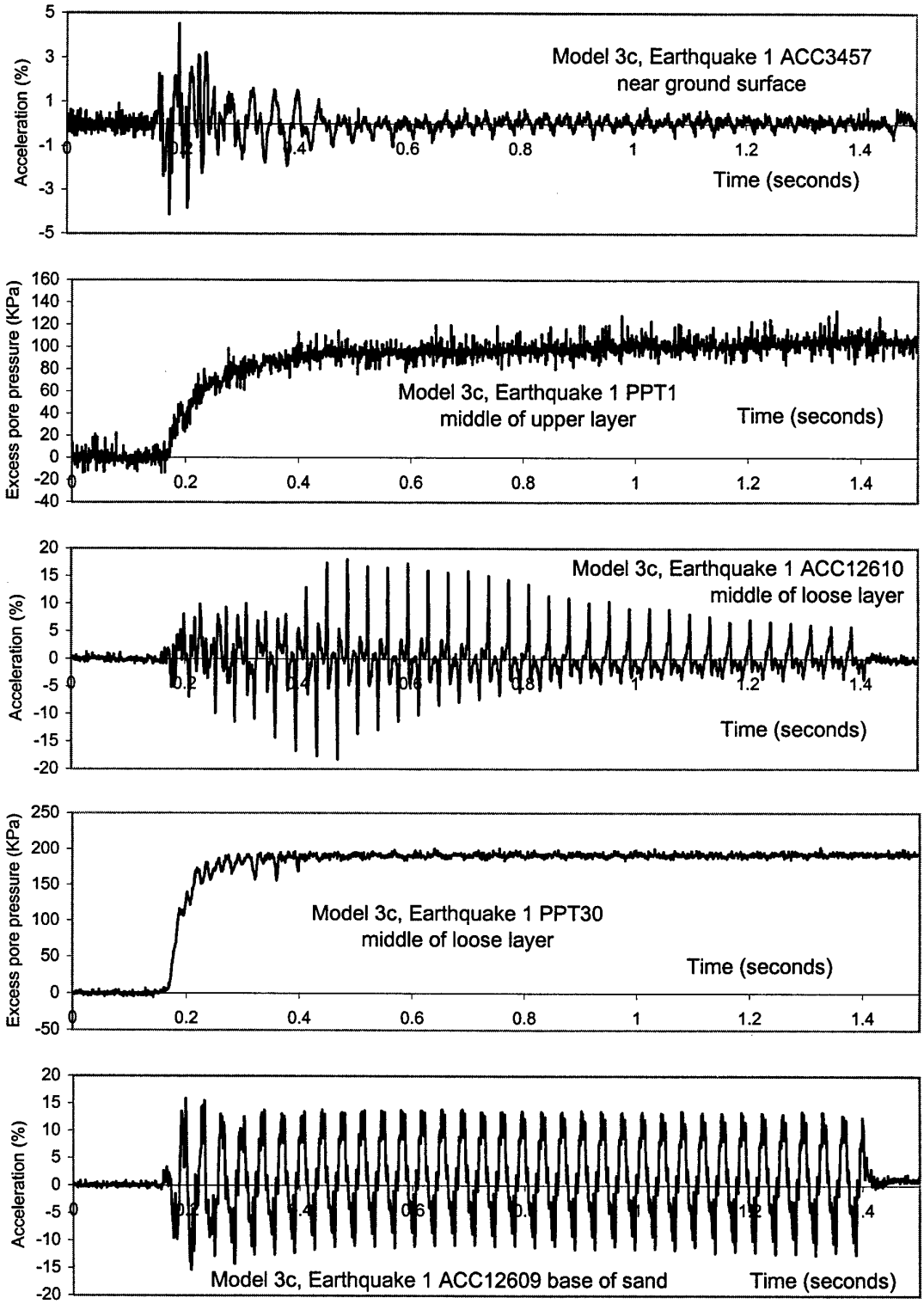

Figure 2.3 Model 3c, Earthquake 1, time histories of acceleration and excess pore pressure

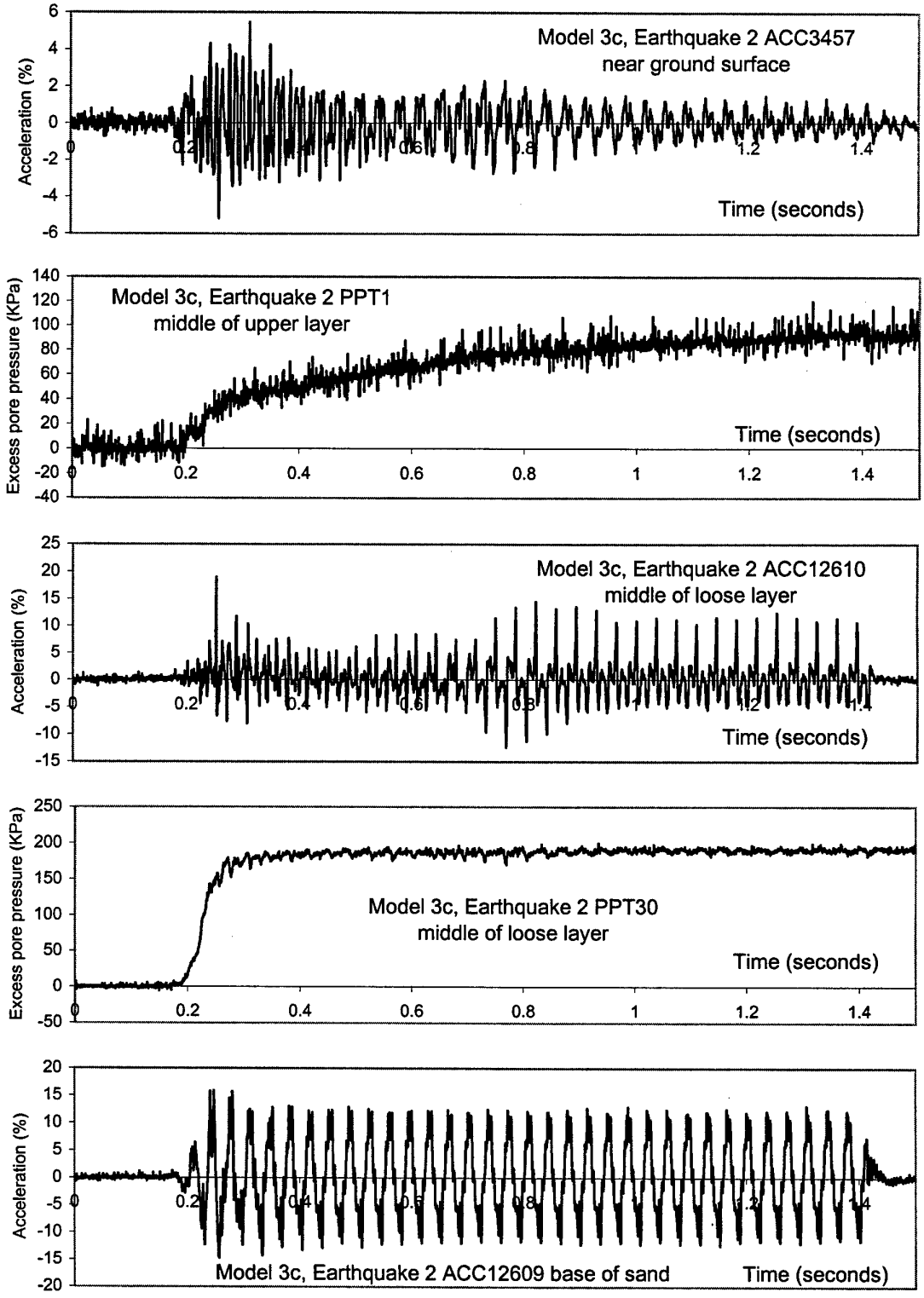

Figure 2.4 Model 3c, Earthquake 2, time histories of acceleration and excess pore pressure

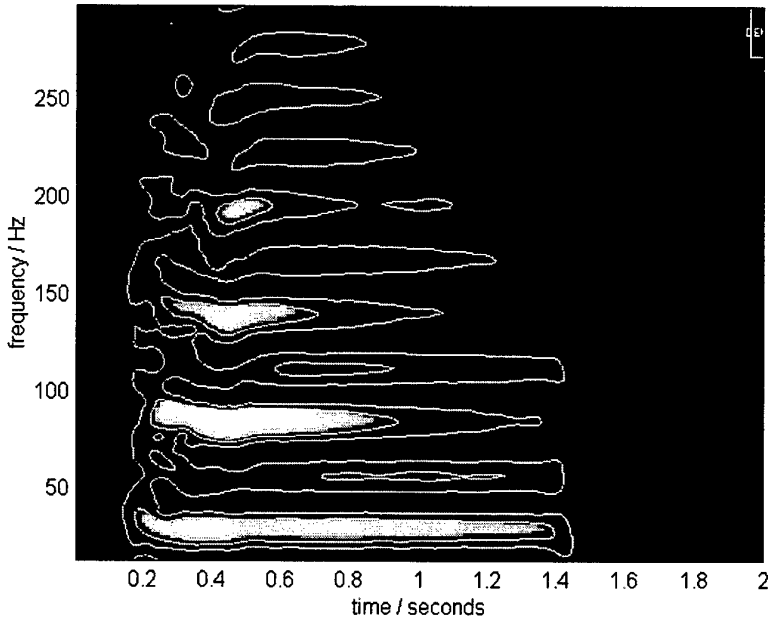

Model 3c, Earthquake 1, ACC12610, middle of loose layer

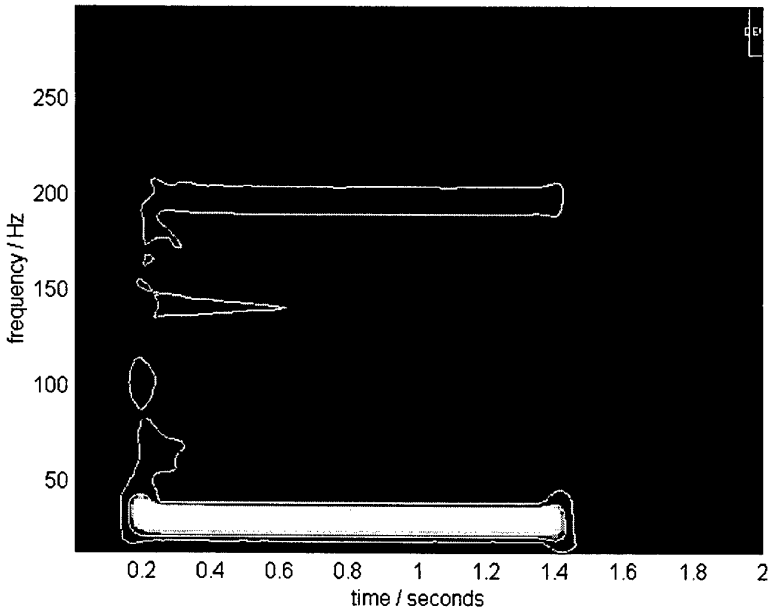

Model 3c, Earthquake 1, ACC12609, base of sand (input motion)

Figure 2.5 Time-frequency maps from Model 3c EQ1

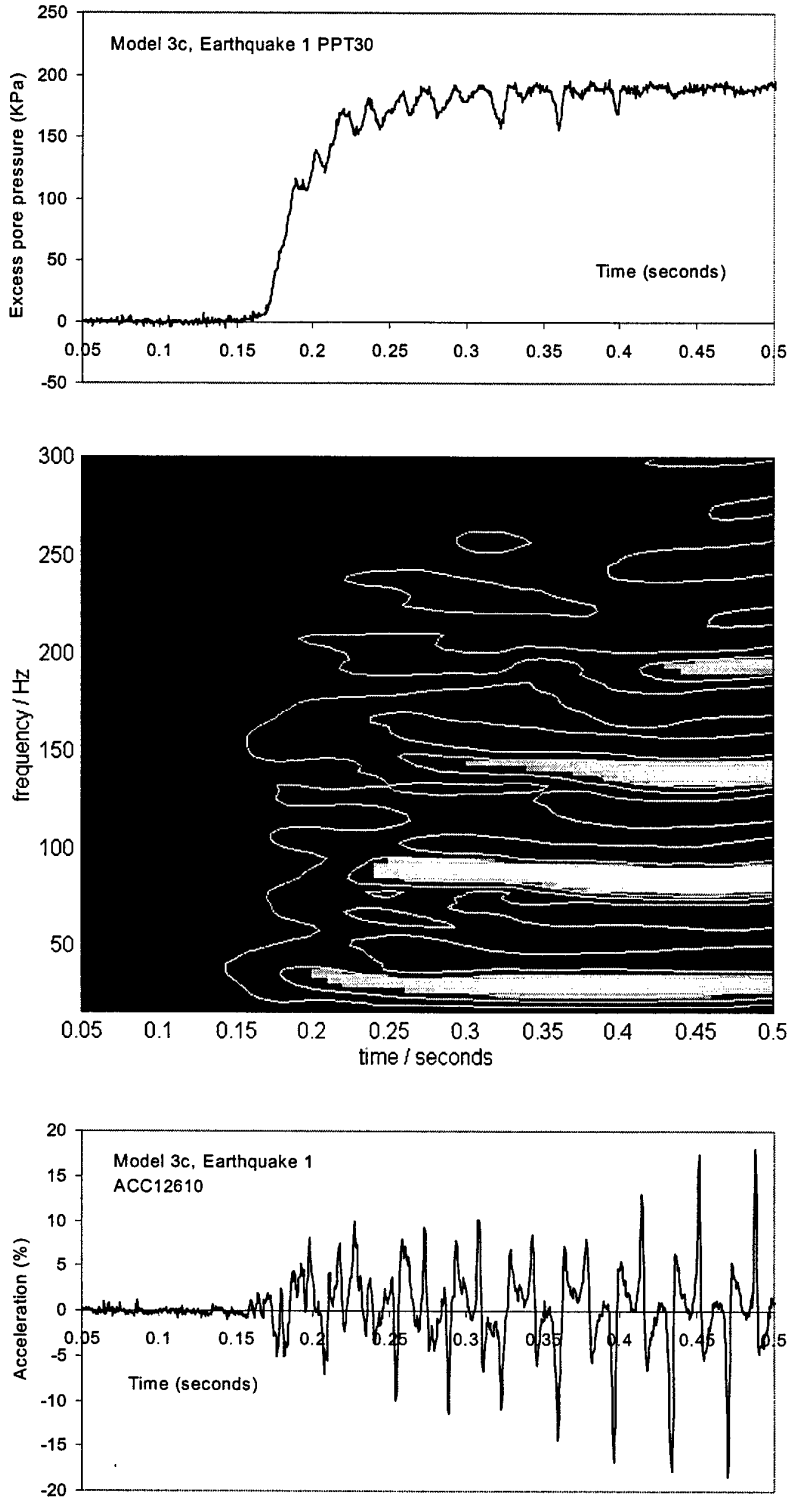

Figure 2.6 Wavelet analysis for accelerometer 12610 and matching pore pressure response, Model 3c EQ1

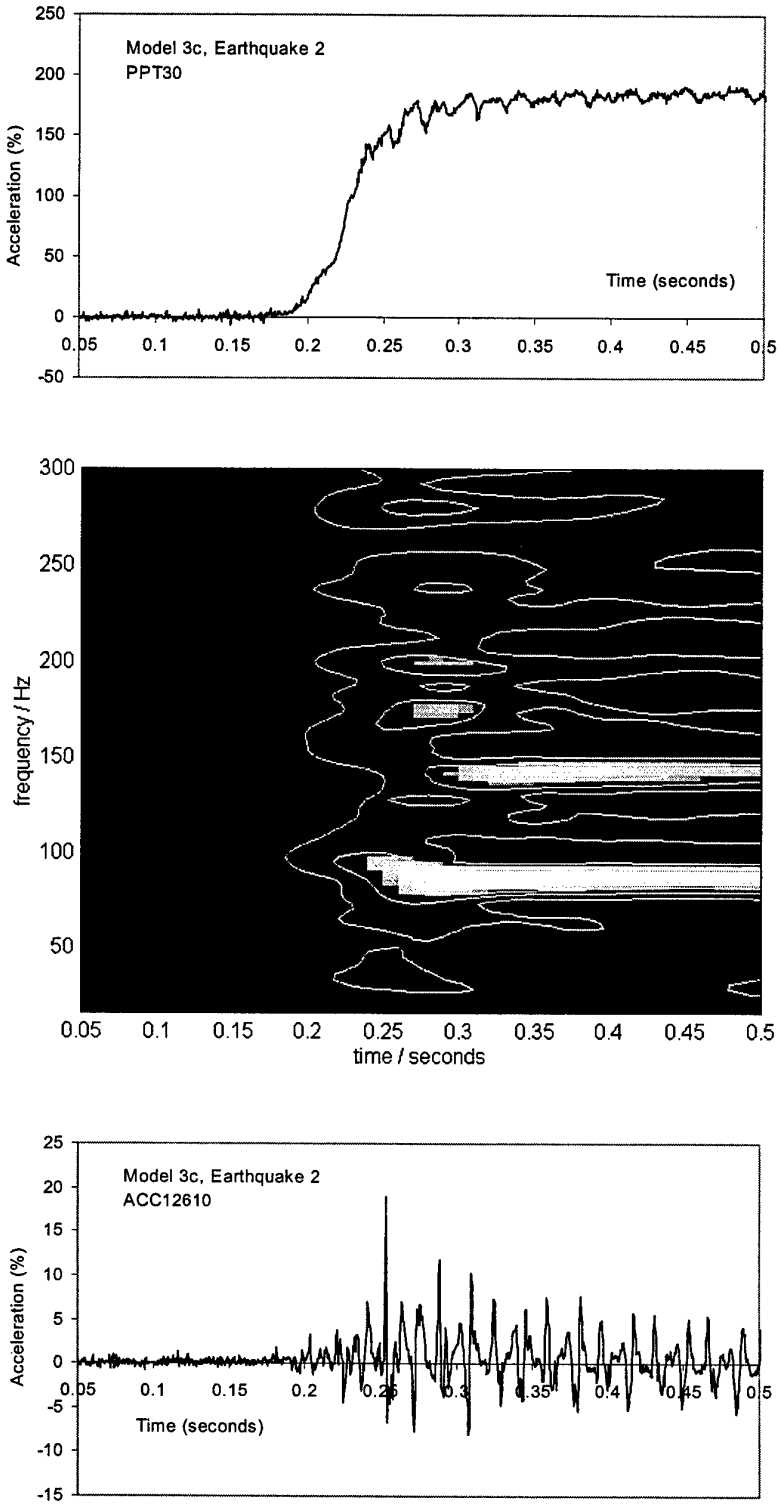

Figure 2.7 Wavelet analysis for accelerometer12610 and matching pore pressure response, Model 3c EQ2

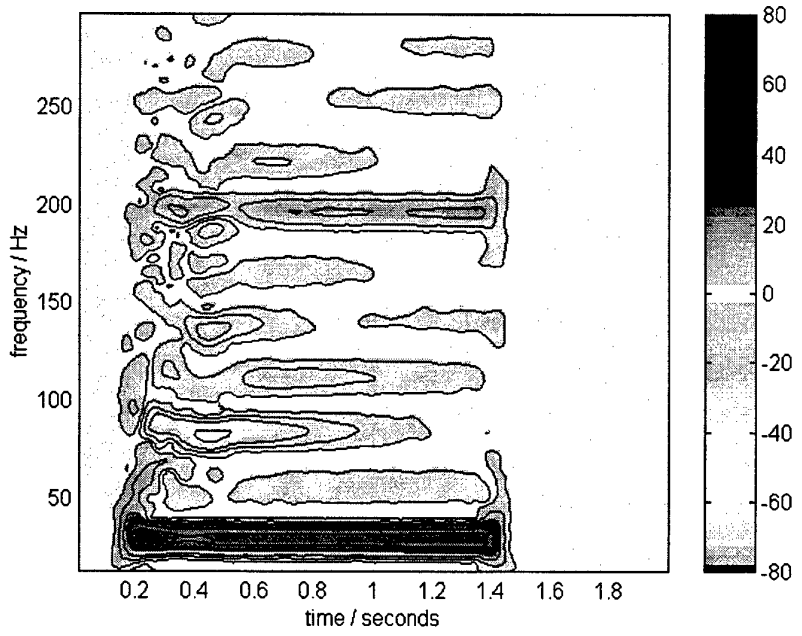

Figure 2.8 Differential time-frequency map of accelerometers 12609(+) and 12610(-) for model 3c EQ1

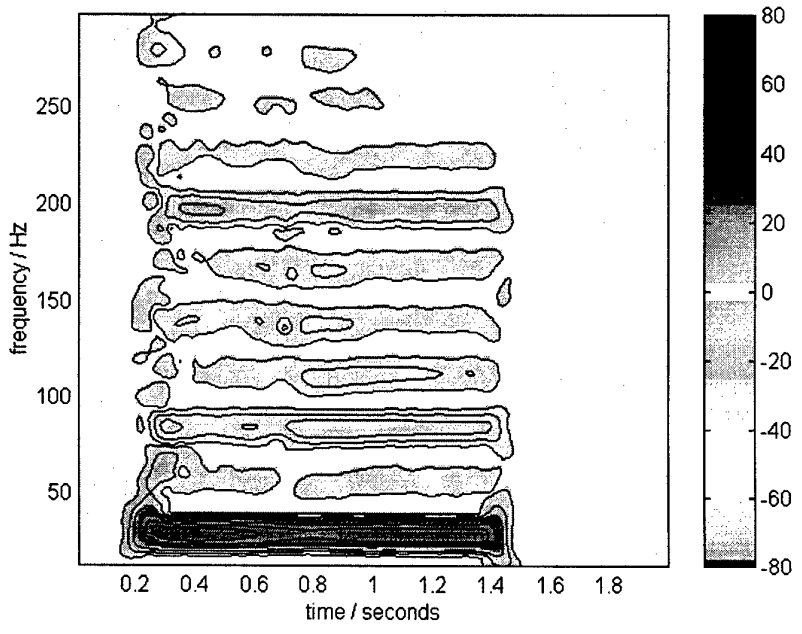

Figure 2.9 Differential time-frequency map of accelerometers 12609(+) and 12610(-) for model 3c EQ2

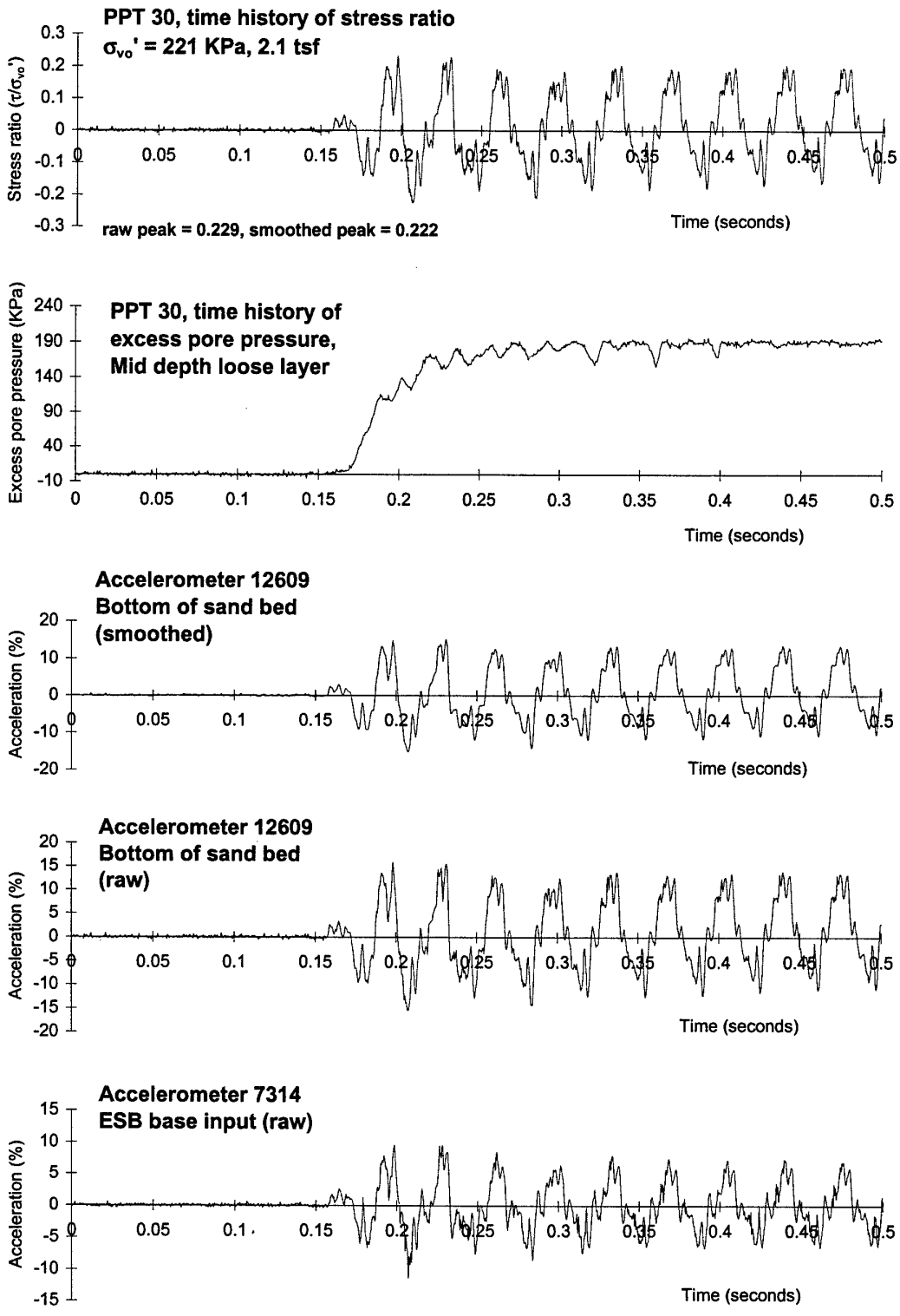

Figure 3.1 Pore pressure transducers and accelerometers, earthquake 1

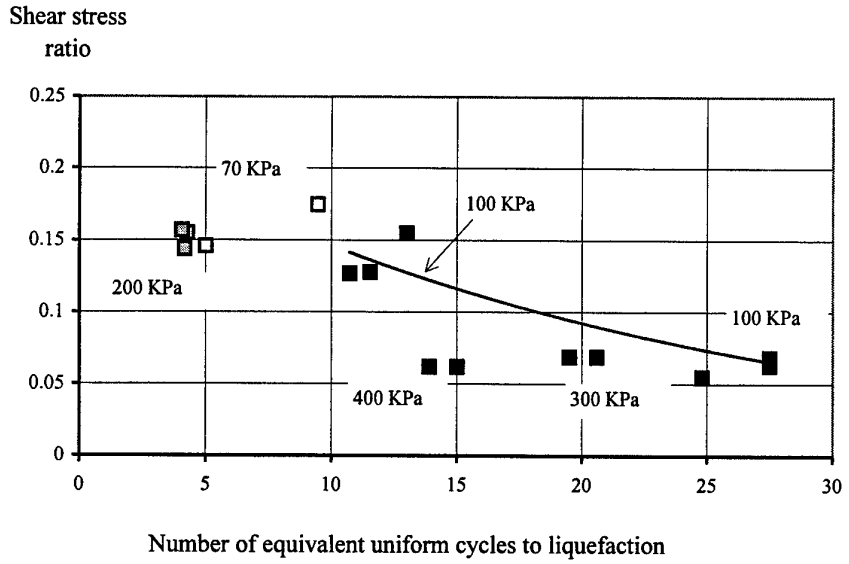

Figure 3.2 Liquefaction data from centrifuge model tests, normally consolidated, first earthquake only, 50% Relative Density

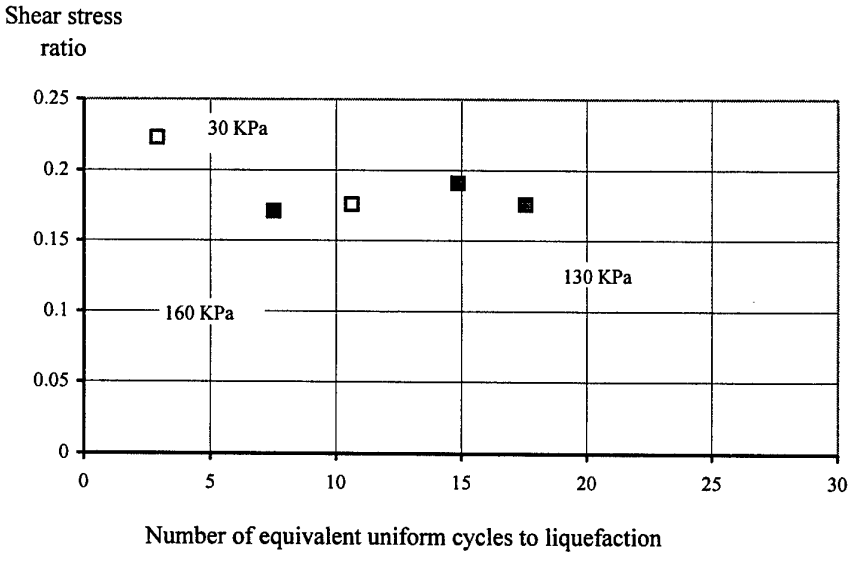

Figure 3.3 Liquefaction data from centrifuge model tests, normally consolidated, first earthquake only, 75% Relative Density

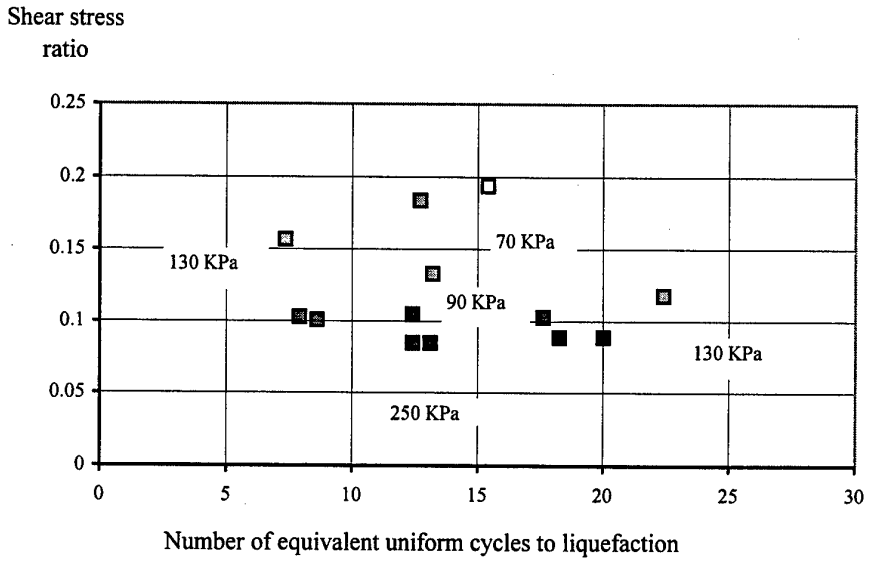

Figure 3.4 Liquefaction data from centrifuge model tests, over consolidated, OCR = 2.25 first earthquake only, 50% Relative Density

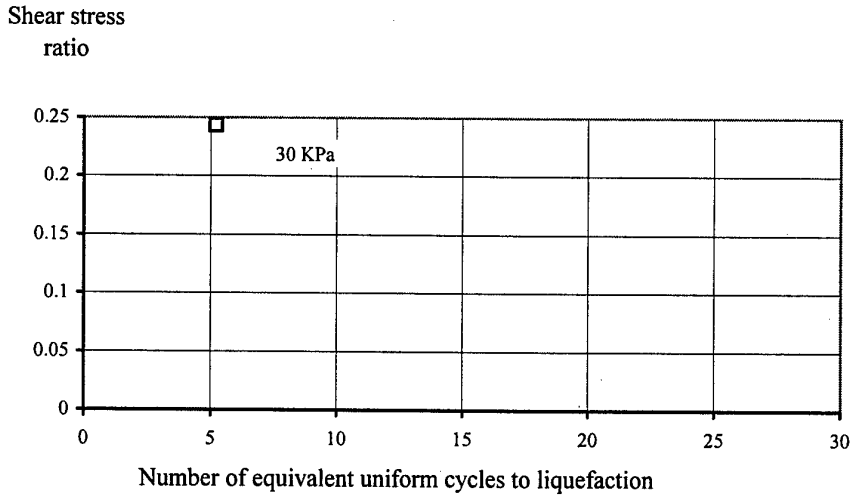

Figure 3.5 Liquefaction data from centrifuge model tests, over consolidated, OCR = 2.25, first earthquake only, 75% Relative Density

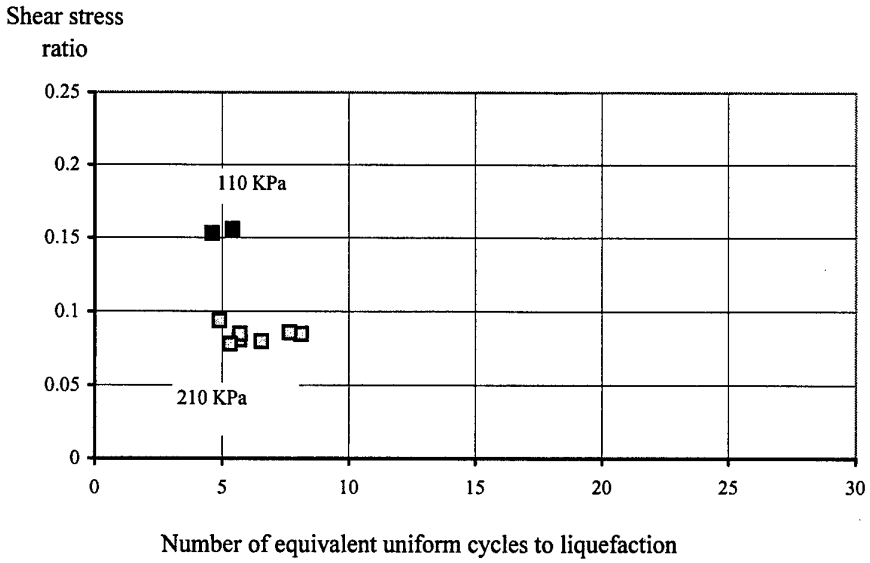

Figure 3.6 Liquefaction data from centrifuge model tests, normally consolidated second and following earthquakes only, 50% Relative Density

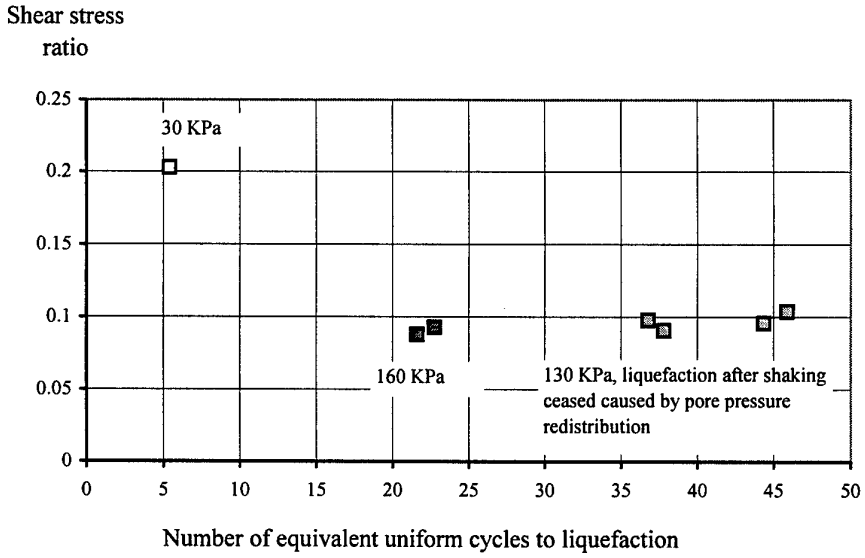

Figure 3.7 Liquefaction data from centrifuge model tests, normally consolidated second and following earthquakes only, 75% Relative Density

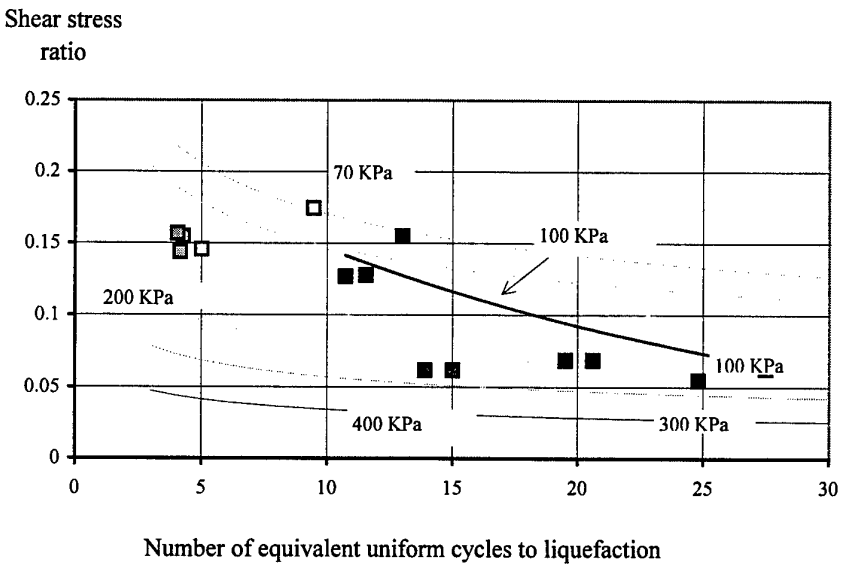

Figure 3.8 Comparison between Figure 2 data and the shape of the liquefaction curves predicted using the Magnitude Scaling Factors of Seed & Idriss

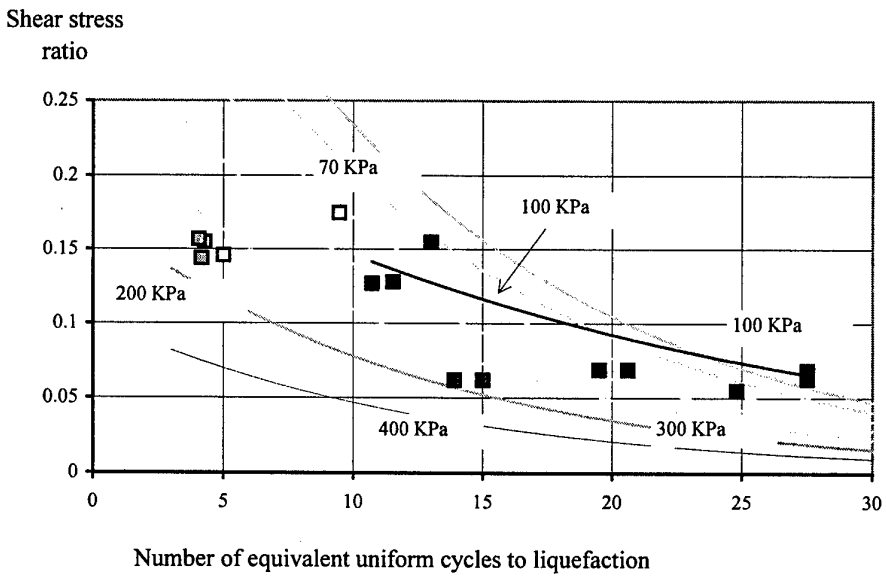

Figure 3.9 Comparison between Figure 2 data and the shape of the liquefaction curves predicted using the Magnitude Scaling Factors by Ambraseys

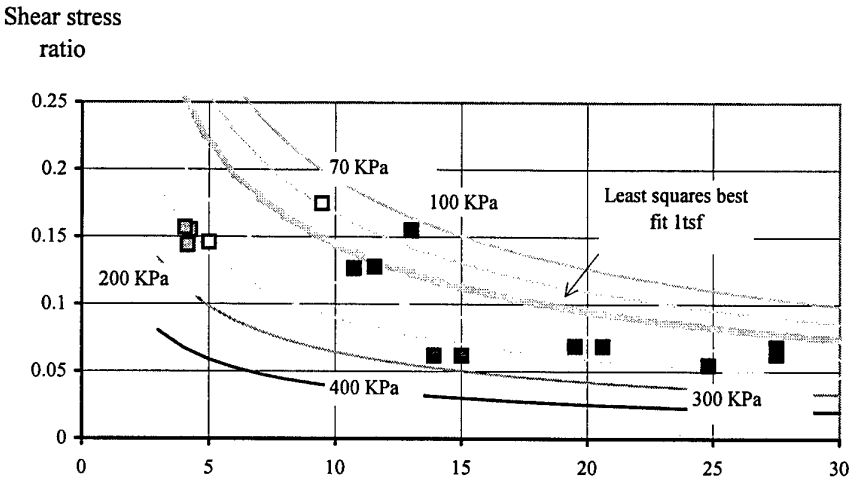

Figure 3.10 Comparison between Figure 2 data and the shape of the liquefaction curves predicted using the Magnitude Scaling Factors by Idriss

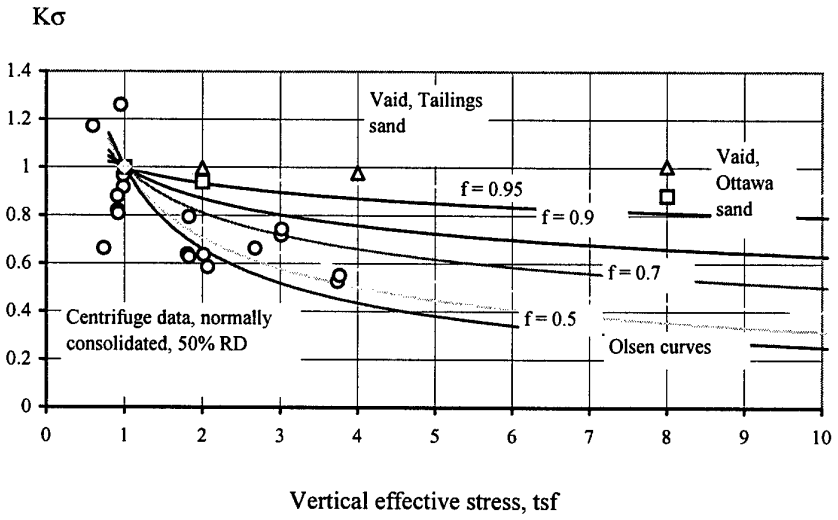

Figure 3.11 Comparison between Figure 2 data expressed as Kσ at 10 cycles, compared with Olsen, 1984 and data from Vaid for Tailings and Ottawa sand

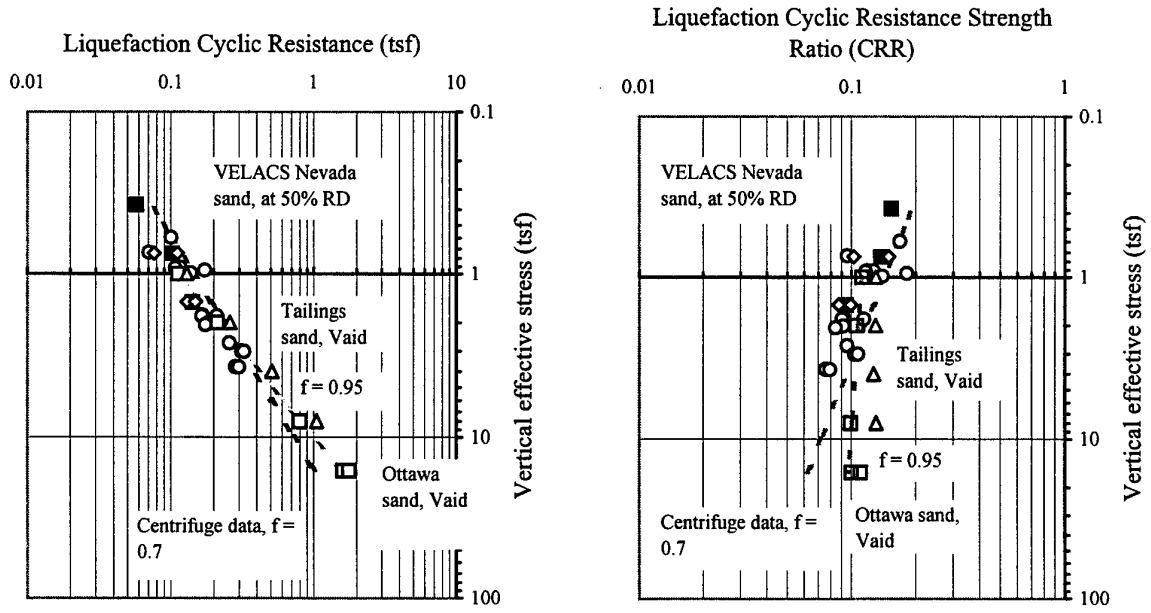

Figure 3.12 Stress focus plots using centrifuge data, normally consolidated, at 50% RD, compared with VELACS laboratory test data on Nevada sand corrected to 50% RD (CIUCyclic solid squares, CSS open diamonds) and 10 cycles, and data from Vaid at 50% RD on Tailings sand and Ottawa sand.

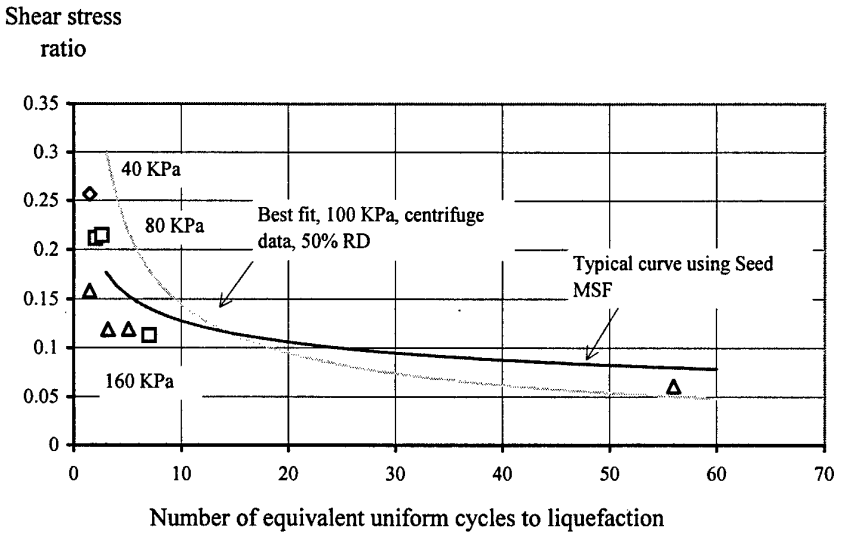

Figure 3.13 Comparison between laboratory data for Nevada sand corrected to 50% RD, the 'best fit' curve predicted using the Idriss Magnitude Scaling Factors at 110KPa, and the shape of typical curves generated using Seed's original MSF

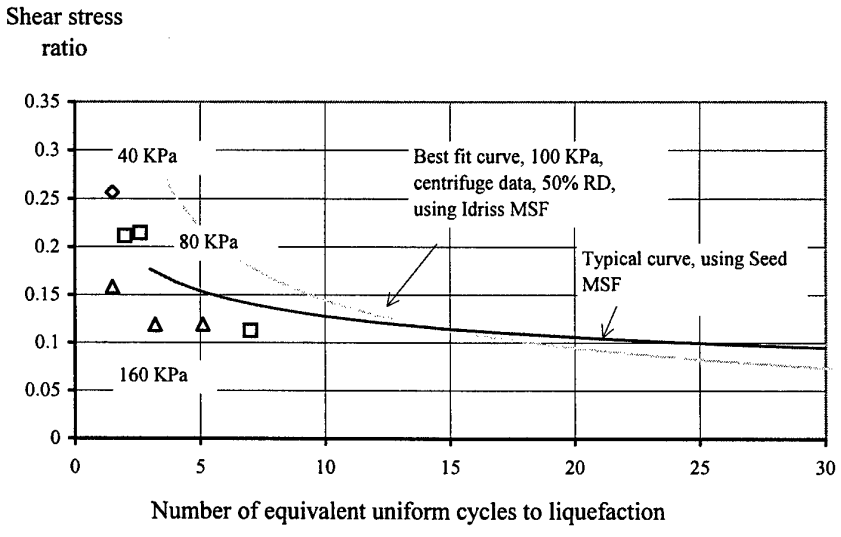

Figure 3.14 Comparison between laboratory data corrected to 50% RD, the 'best fit' curve predicted using the Idriss Magnitude Scaling Factors at 110KPa, and a typical curve using Seed's original MSF, at less than 30 cycles

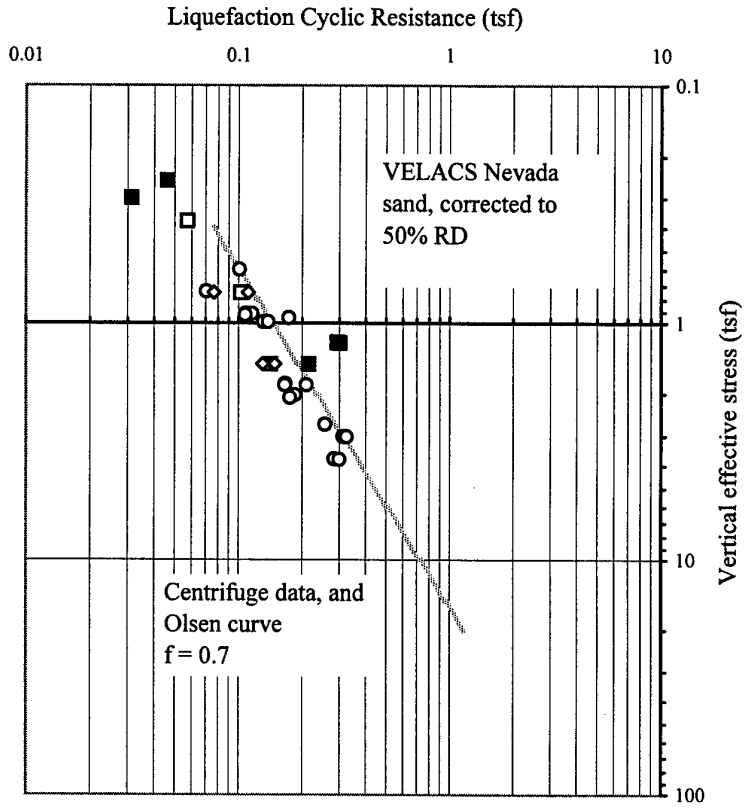

Figure 3.15 Stress focus plot using centrifuge data, normally consolidated, 50% and 75% RD, computed for 10 cycles using Idriss MSF, and compared with VELACS laboratory test data on Nevada sand corrected to 50% RD (CIUCyclic open squares, CSS open diamonds) and projected to 10 cycles using Seed MSF. Centrifuge data of 50% RD open circles, and 75% RD, solid squares.

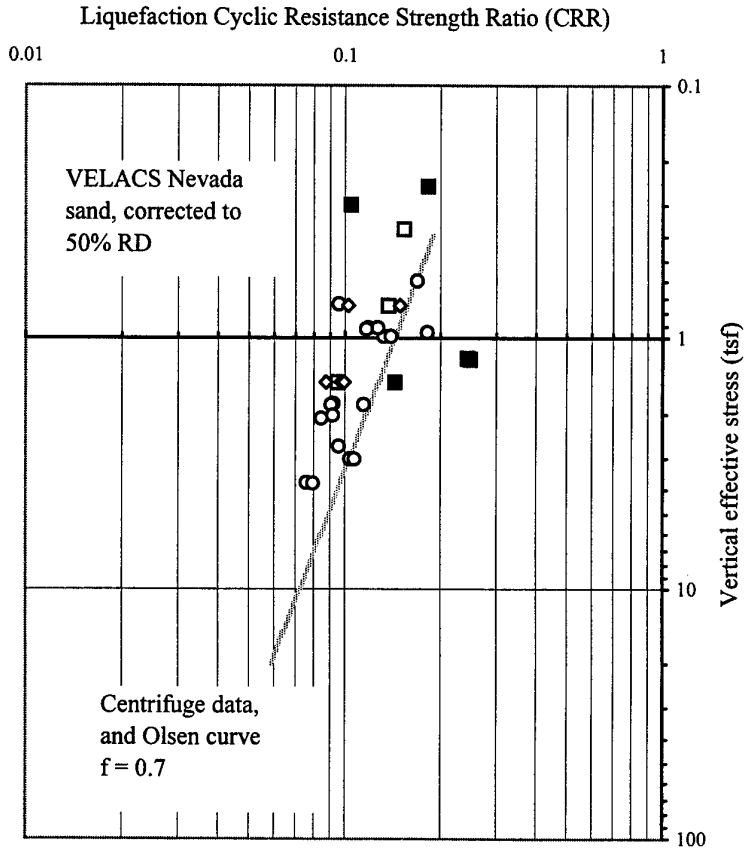

Figure 3.16 Stress focus plot using centrifuge data, normally consolidated, 50% and 75% RD, computed using Idriss MSF for 10 cycles, and compared with VELACS laboratory test data on Nevada sand corrected to 50% RD (CIUCyclic open squares, CSS open diamonds) and projected to 10 cycles using Seed MSF. Centrifuge data 50%, open circles, and 75% RD, solid squares.

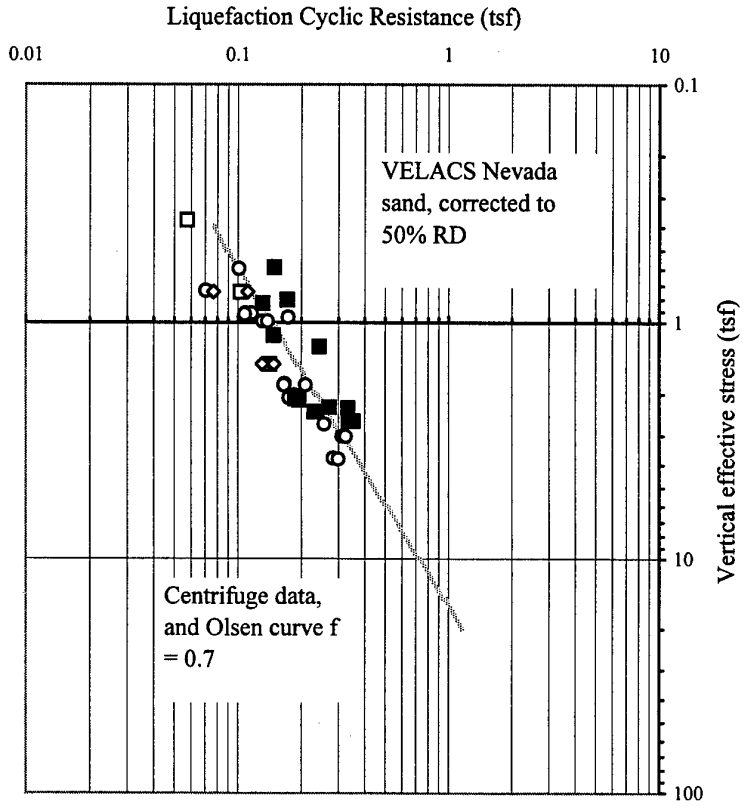

Figure 3.17 Stress focus plot using centrifuge data, normally and overconsolidated, at 50%, computed for 10 cycles using Idriss MSF, and compared with VELACS laboratory test data on Nevada sand corrected to 50% RD (CIUCyclic open squares, CSS open diamonds) and projected to 10 cycles using Seed MSF. Centrifuge data of normally consolidated specimens open circles, and overconsolidated (OCR = 2.25), solid squares.

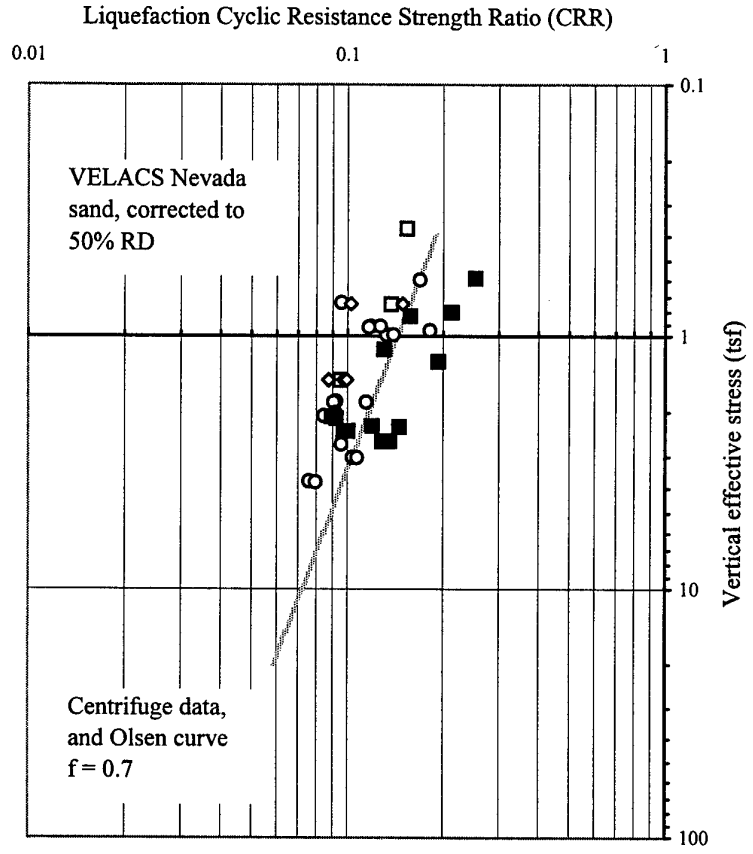

Figure 3.18 Stress focus plot using centrifuge data, normally and overconsolidated, at 50% RD, computed using Idriss MSF for 10 cycles, and compared with VELACS laboratory test data on Nevada sand corrected to 50% RD (CIUCyclic open squares, CSS open diamonds) and projected to 10 cycles using Seed MSF. Centrifuge data normally consolidated 50% RD, open circles, overconsolidated 50% RD solid squares.

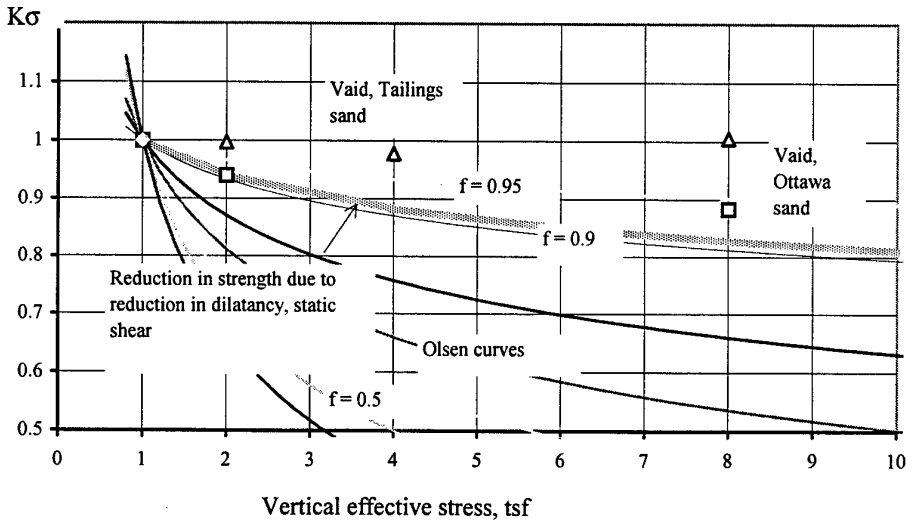

Figure 4.1 Comparison between Olsen 'curves', 1984 and data from Vaid for Tailings and Ottawa sand, and reduction in strength in static shearing

APPENDIX A

GLYCERINE WATER MIXTURES
MEASURED PROPERTIES

N J McCullough, WES, 10-11 December 1998

% glycerin by weight	Temp	Viscosity (cS)				Density	Temp
	(deg C)	Low	High	Average	Spread	(gm/cm3)	(deg C)
0	6	1.5	1.5	1.5	0.0	1.00	19.5
	8.5	1.3	1.4	1.4	0.0		
	12	1.0	1.0	1.0	0.0		
	16.3	1.0	1.0	1.0	0.0		
	25	1.0	1.0	1.0	0.0		
49.9	12	12.9	13.1	13.0	0.1	1.11	19.5
	16	10.0	11.0	10.5	0.5		
	20.5	7.8	8.5	8.2	0.4		
	24.5	6.5	7.0	6.8	0.3		
	30.5	4.5	4.8	4.7	0.1		
65	8	27.2	27.6	27.4	0.2	1.16	23.5
	9.5	24.2	24.5	24.4	0.1		
	14.0	20.5	20.8	20.7	0.2		
	15.0	19.5	20.0	19.8	0.3		
	21.0	17.5	17.9	17.7	0.2		
	23.5	17.0	18.0	17.5	0.5		
	29.0	15.5	16.0	15.8	0.3		
	33.0	14.0	14.5	14.3	0.3		
75	2.5	105.0	107.0	106.0	1.0		
	5.0	90.0	92.0	91.0	1.0		
	10.0	67.0	69.0	68.0	1.0		
	15.0	51.0	52.0	51.5	0.5		
	21.5	35.0	37.0	36.0	1.0		
	28.5	23.2	23.5	23.4	0.1		
	35.5	18.1	18.5	18.3	0.2		
85.6	6.0	275.0	280.0	277.5	2.5	1.21	20.0
	8.0	203.0	208.0	250.5	2.5		
	12.0	154.0	158.0	156.0	2.0		
	15.0	135.0	136.0	135.5	0.5		
	17.5	114.0	116.0	115.0	1.0		
	20.5	97.0	98.0	97.5	0.5		
	22.0	85.0	86.0	85.5	0.5		
	22.3	87.5	89.0	88.3	0.8		
	25.0	75.0	77.0	76.0	1.0		
	25.5	72.5	74.0	73.3	0.8		
	33.0	49.0	51.0	50.0	1.0		

APPENDIX B

Summary of liquefaction data

Data of liquefaction, Models and cycles

Model, Earthquake	Eq	Peak acc'n	Overburden (KPa)	Cycles to liquef'n	Stress ratio	Relative Density (%)	Quality low/med/high/*	PPT	Comments
Data of liquefaction in first earthquakes, at 50% relative density									
Model 2d, 1	1	50	64	9.45	0.175	50	*	3	Excellent, high spike omitted
Model 2d, 1	1	50	79	5	0.146	50	*	31	Excellent, high spike omitted, some arching
Model 2b, 1	1	50	106	10.719	0.127	50	*	10	Excellent, although double smoothed for high frequencies
Model 2c, 1	1	50	98	27.5	0.064	49	high	46	Data cut off before full liquefaction could be observed
Model 2c, 1	1	50	98	27.5	0.0685	49	high	41	PPT41 seems to be very close to 100% at the end of the eq
Model 2b, 1	1	50	106	11.529	0.128	50	*	30	Excellent, although double smoothed for high frequencies
Model 2c, 1	1	50	99	27.5	0.063	49	med	49	Data cut off before full liquefaction could be observed
Model 2d, 1	1	50	102	13	0.155	50	high	46	High static pore pressure; high spike omitted, some arching
Model 3c, 1	1	50	194	4.266	0.155	50	*	30	Excellent
Model 3a, 1	1	50	196	4.185	0.195	34	med	9	Spikey acceleration record
Model 3c, 1	1	50	196	4.05	0.157	50	*	31	
Model 3a, 1	1	50	216	3.78	0.166	34	med	10	Concern over high static pore pressure value
Model 3c, 1	1	50	222	4.16	0.144	50	*	10	Excellent
Model 4a, 1	1	50	287	24.8	0.055	49	high	45	Definition of 100% not clear, high spike at beginning
Model 4c, 1	1	50	323	19.5	0.069	50	high	51	Arching of surcharge
Model 4c, 1	1	50	324	20.6	0.069	50	high	38	Arching of surcharge
Model 5a, 1	1	50	401	13.9	0.062	51	high	51	Arching of surcharge
Model 5a, 1	1	50	404	15	0.062	51	high	38	Arching of surcharge
Data of liquefaction in first earthquakes, at 75% relative density									
Model 2b, 1	1	50	27	10.611	0.176	75	*	31	Excellent, although double smoothed for high frequencies
Model 2a, 1	1	50	30	2.51	0.194	83	low		Model 2a, eqs 1,2 and 3 showed liquefaction in dense layer only. No static pwp
Model 1a, 1	1	50	34	10.8	0.081	70	med	31	Model 1a; some uncertainty over measured depth of transducers afterwards,
Model 2d, 1	1	50	32	2.89	0.223	75	high	7	High static pore pressure, spike at beginning omitted
Model 3c, 1	1	50	130	17.55	0.176	75	high	11	Liquefaction could be earlier
Model 3c, 1	1	50	129	14.85	0.191	75	high	16	Liquefaction could be earlier
Model 3c, 1	1	50	160	7.506	0.171	75	high	15	Rapid rise time, liquefaction could be earlier
Data of liquefaction in second and following earthquakes, at 50% relative density									
Model 2b, 2	2	50	111	5.4	0.156	50	high	10	Large pulse at beginning, but left because of rapid rise time
Model 2b, 2	2	50	115	4.59	0.153	50	high	30	Large pulse at beginning, but left because of rapid rise time
Model 3b, 3	3	50	190	5.157	0.095	50	med	16	Calibration uncertain
Model 3c, 2	2	50	194	6.534	0.08	50	high	30	Could be 1 or 2 cycles earlier
Model 3c, 3	3	50	194	8.1	0.085	50	high	30	Could be 3 or 4 cycles earlier
Model 3a, 2	2	50	199	7.911	0.184	34	low	9	Slow buildup very different
Model 3c, 2	2	50	196	5.67	0.081	50	high	31	Could be 1 or 2 cycles earlier
Model 3c, 3	3	50	196	7.641	0.086	50	high	31	Could be 3 or 4 cycles earlier
Model 3a, 2	2	50	213	3.591	0.16	34	med	10	and spikey acceleration record
Model 3b, 2	2	50	198	5.427	0.086	50	med	16	Calibration uncertain
Model 3b, 3	3	50	197	4.887	0.094	50	high	2	Liquefaction could be earlier
Model 3b, 2	2	50	200	5.697	0.085	50	high	2	Liquefaction could be earlier
Model 3c, 2	2	50	222	19.494	0.074	50	med	10	Double stage rise curious
Model 3c, 3	3	50	222	15.309	0.079	50	med	10	Double stage rise, again
Model 3b, 2	2	50	228	5.292	0.078	50	high	11	Slightly low output
Model 5a, 2	2	50	348	30.9	0.067	51	med	51	Lower level than eq 1 suggests may not be 100%
Model 5a, 2	2	50	348	30.9	0.067	51	med	38	Lower level than eq 1 suggests may not be 100%
Model 5c, 3	3	50	974	28.5	0.0427	52	low	41	Possible arching
Model 5c, 3	3	50	1009	27.3	0.04	52	low	51	Possible arching

Data of liquefaction in second and following earthquakes, at 75% relative density

Model 2b, 2	2	50	32	5.4	0.203	75	high	31 Large spike at beginning of eq may distort peak accn
Model 2a, 2	2	50	30	2.48	0.152	83	low	readings, so estimated values used. Estimates based on acc's only.
Model 2a, 3	3	50	30	3.4	0.16	83	low	
Model 1a, 2	2	50	35	12.4	0.0511	70	med	31 also max pwp seems low. Second eq showed slow rise from 90-100%
Model 3c, 2	2	50	130	37.8	0.091	75	high	11 Could be up to 5 cycles earlier
Model 3c, 3	3	50	130	44.33	0.096	75	high	11 Could be up to 10-11 cycles earlier
Model 3c, 2	2	50	129	36.774	0.098	75	high	16 Could be up to 5 cycles earlier
Model 3c, 3	3	50	129	45.87	0.104	75	high	16 Could be up to 12 cycles earlier
Model 3c, 2	2	50	160	21.6	0.088	75	high	15 Good definition of 100%
Model 3c, 3	3	50	160	22.734	0.093	75	high	15 Good

Data of liquefaction in first earthquakes, at 50% relative density, overconsolidated OCR = 2.25

Model 2e, 1	1	125	60	13.4	0.151	49	med	52 Kink in pore pressure generation time history, static readings at 50g unreliable
Model 2f, 1	1	125	63	15.4	0.194	50	high	31 Liquefaction could be 1.5 cycles earlier
Model 2f, 1	1	125	86	12.7	0.184	50	*	47 Excellent, some arching
Model 2e, 1	1	125	89	13.2	0.133	49	high	47 Static readings at 50g not totally reliable
Model 2f, 1	1	125	121	7.34	0.157	50	*	46 Excellent, some arching
Model 2e, 1	1	125	135	22.4	0.118	49	high	49 Static readings at 50g not totally reliable
Model 3d,1	1	125	223	7.9	0.103	54	*	40 Excellent
Model 3d, 1	1	125	226	8.6	0.101	54	*	48 Excellent
Model 3d, 1	1	125	245	17.6	0.103	54	high	37 Slow buildup makes definition of 100% difficult
Model 3d, 1	1	125	243	12.4	0.105	54	high	35 Slow buildup makes definition of 100% difficult
Model 4d,1	1	125	254	13.1	0.085	50	high	38 Arching of surcharge
Model 4d,1	1	125	254	12.4	0.085	50	high	51 Arching of surcharge
Model 5b, 1	1	125	278	20	0.089	49	high	51 Arching of surcharge
Model 5b, 1	1	125	279	18.25	0.089	49	high	38 Arching of surcharge

Data of liquefaction in second and following earthquakes, at 50% relative density, overconsolidated OCR = 2.25

Model 4b, 2	2	125	369	24.4	0.109	56	med	39 Use double smoothing to address high frequencies
Model 3d, 2	2	125	213	14.8	0.124	54	med	37 Very rapid rise to 90%, slow build to 100%
Model 3d, 2	2	125	203	11.8	0.131	54	med	35 Very rapid rise to 90%, slow build to 100%
Model 3d, 3	3	125	208	8	0.129	54	med	37 Very rapid rise to 90%, slow build to 100%
Model 3d, 3	3	125	198	8.5	0.136	54	med	35 Very rapid rise to 90%, slow build to 100%
Model 3d, 4	4	125	193	28.6	0.143	54	med	37 Very rapid rise to 90%, slow build to 100%
Model 3d, 4	4	125	198	27.2	0.145	54	med	35 Very rapid rise to 90%, slow build to 100%
Model 3d, 4	4	125	182	28.1	0.138	54	med	48 Possible arching
Model 3d, 4	4	125	182	25.9	0.139	54	med	40 Possible arching

Data of liquefaction in first earthquakes, at 75% relative density, overconsolidated OCR = 2.25

Model 2f, 1	1	125	32.2	5.21	0.244	75	*	38 Excellent

APPENDIX C

CALCULATION OF LIQUEFACTION CURVE BASED ON LABORATORY DATA OF NEVADA SAND

References:

Arumoli, K, Muraleetharan, KK, Hossain M M and Fruth L S (1992), VELACS Verification of Liquefaction Analyses by Centrifuge Studies Laboratory Testing Program Soil Data Report, report for the National Science Foundation, Earth Technology Corporation, Irvine CA, Project No. 90-0562, March.

Popescu R and Prevost J H (1993) Numerical class 'A' predictions for Models Nos 1, 2, 3, 4a, 4b, 6, 7, 11 & 12, Proc Int Conf Verification Numerical Procedures for the Analysis of Soil Liquefaction Problems, Davis, Arulanandan & Scott (eds) CA, 17 - 20 October, pp 1105 - 1207, AA Balkema.

Data selected based on isotropic consolidation, without initial shear offset

Test	RD	Test	Fig	σ'_3, σ'_v	q, τ	Cycles	converting triaxial to simple shear Popescu & Prevost, eq (5) τ/σ'_v	tsf	τ
CIUCyclic	60	60-88	4-21a	40	24.4	1.5	0.352184	0.372953	0.131348
CIUCyclic	60	60-86	4-26a	80	40.3	2	0.29084	0.745907	0.21694
CIUCyclic	60	60-87	4-27a	160	60.2	1.5	0.217228	1.491814	0.324064
CSS	60	60-05	4-37a	80	12.4	7	0.155	0.745907	0.115616
CSS	60	60-04	4-38a	80	23.6	2.6	0.295	0.745907	0.220043
CSS	60	60-07	4-39a	160	13.4	56	0.08375	1.491814	0.124939
CSS	60	60-06	4-40a	160	26.1	3.2	0.163125	1.491814	0.243352
CSS	60	60-08	4-41a	160	26.2	5.1	0.16375	1.491814	0.244284

Correction for 50% RD

From Relative density vs Nspt vs stress, Holtz W G and Gibbs H J (1979) SPT and relative density in coarse sand, J Geotech Div, ASCE, 105 GT3, pp439-441

N =	10	blows at	50% RD
	13.4		60%
	19		70%

From Seed's figure for Mag 7.5 earthquake correlating cyclic stress ratio with modified penetration resistance,

CSR =	0.102	50%
	0.14	60%
	0.19	70%

Hence scale the CSR by 0.728571 to convert from 60% to 50%.

Test	Corrected	Test	σ'_3, σ'_v	q, τ	Cycles	Original (60%) τ/σ'_v	tsf	Corrected (50%) τ/σ'_v	τ
CIUCyclic	50%	60-88	40	24.4	1.5	0.352184	0.372953	0.256591	0.095696
CIUCyclic	50%	60-86	80	40.3	2	0.29084	0.745907	0.211898	0.158056
CIUCyclic	50%	60-87	160	60.2	1.5	0.217228	1.491814	0.158266	0.236104
CSS	50%	60-05	80	12.4	7	0.155	0.745907	0.112929	0.084234
CSS	50%	60-04	80	23.6	2.6	0.295	0.745907	0.214929	0.160317
CSS	50%	60-07	160	13.4	56	0.08375	1.491814	0.061018	0.091027
CSS	50%	60-06	160	26.1	3.2	0.163125	1.491814	0.118848	0.177299
CSS	50%	60-08	160	26.2	5.1	0.16375	1.491814	0.119304	0.177979

Now scale to 10 cycles, to get CSR and CS

Use MSF to deduce CSR at 10 cycles, based on actual data above as follows:

stressratioN = stressratio15*A*N^B, and

stressratio10=stressratio15*A*10^B, then

stressratio10=stressratioN*10^B/N^B

						Idriss A	Idriss B	Seed A	Seed B
						5.2445	-0.6103	2.1206	-0.2707
		overburd tsf	corrected stress ratio	N cycles		CSR at 10cycles	CS (tsf)	CSR at 10cycles	CS (tsf)
CIUCyclic	60-88	40	0.372953	0.256591	1.5	0.080614	0.030065	0.153536	0.057262
CIUCyclic	60-86	80	0.745907	0.211898	2	0.07935	0.059187	0.137061	0.102235
CIUCyclic	60-87	160	1.491814	0.158266	1.5	0.049723	0.074177	0.094701	0.141277
CSS	60-05	80	0.745907	0.112929	7	0.090838	0.067757	0.102535	0.076482
CSS	60-04	80	0.745907	0.214929	2.6	0.094461	0.070459	0.149255	0.11133
CSS	60-07	160	1.491814	0.061018	56	0.174613	0.26049	0.097273	0.145113
CSS	60-06	160	1.491814	0.118848	3.2	0.059291	0.08845	0.087305	0.130242
CSS	60-08	160	1.491814	0.119304	5.1	0.079101	0.118004	0.099424	0.148323